International Journal of Biological Macromolecules 354 (2026) 151333

Contents lists available at ScienceDirect

International Journal of Biological Macromolecules

journal homepage: www.elsevier.com/locate/ijbiomac

Structural and functional investigation of RD3-GCAP1 interaction in retinal photoreceptors under normal and disease conditions

Valerio Marino [a], Effibe O. Ahoulou [b], Giuditta Dal Cortivo [a], Anna Avesani [a], James B. Ames [b], Daniele Dell'Orco [a,*]

[a] Department of Neurosciences, Biomedicine and Movement Sciences, Section of Biological Chemistry, University of Verona, 37134, Verona, Italy
[b] Department of Chemistry, University of California, Davis, CA, 95616, USA

ARTICLE INFO

Keywords:
GCAP1
RD3
Guanylate cyclase
Calcium
Phototransduction
Retinal dystrophy
Protein-protein interaction

ABSTRACT

Guanylate Cyclase Activating Protein 1 (GCAP1) and Retinal Degeneration Protein 3 (RD3) are key regulators of retinal guanylate cyclase 1 (GC1), whose dysregulation leads to inherited retinal dystrophies (IRDs). While GCAP1 mutations cause constitutive GC1 activation and photoreceptor degeneration, RD3 acts as a potent cyclase inhibitor essential for proper GC1 trafficking. Here, we investigated the molecular interaction between GCAP1 and RD3 as well as its perturbation by IRD-associated GCAP1 mutations (D100G, N104H, E111V, E155G) using NMR spectroscopy, surface plasmon resonance, AlphaFold3 modeling, enzymatic assays, and their localization via immunohistochemistry. The results demonstrate that the GCAP1-RD3 interaction is strongly Ca^{2+}-dependent, with Ca^{2+}-bound GCAP1 exhibiting micromolar affinity for RD3 ($K_D \sim 1.6$ μM) and Mg^{2+}-bound GCAP1 showing much weaker binding. Strikingly, the E111V mutation completely abolishes RD3 binding, whereas other variants retain interaction with differential kinetic properties. AlphaFold3 modeling, validated by NMR data, reveals that GCAP1 residues involved in RD3 binding overlap with those residues that mediate GCAP1 dimerization and GC1 interaction. Functional assays demonstrate that RD3 inhibits GC1 cyclase activity through dual mechanisms: direct binding to GC1 and GCAP1-mediated inhibition. Remarkably, RD3 rescues GC1 dysregulation caused by all tested GCAP1 mutations, regardless of their ability to interact with RD3. Immunohistochemistry reveals co-localization of GCAP1, RD3, and GC1 in photoreceptor inner segments and synaptic terminals, where Ca^{2+} concentrations favor complex formation. Our findings suggest that the Ca^{2+} gradient across the connecting cilium acts as a biochemical switch controlling RD3-GCAP1 interaction, and support RD3-based protein delivery as a mutation-independent therapeutic strategy for GCAP1-associated retinal dystrophies.

1. Introduction

Vertebrate phototransduction relies on precise spatiotemporal regulation of cyclic guanosine monophosphate (cGMP) levels in rod and cone photoreceptors. Light absorption by visual pigments triggers the activation of phosphodiesterase 6, which hydrolyzes cGMP, leading to closure of cyclic nucleotide-gated channels and a consequent drop in intracellular Ca^{2+} concentration from ~ 500 nM in darkness to below 50 nM under bright illumination [1]. The restoration of cGMP levels during recovery from light exposure is achieved by retinal guanylate cyclases, predominantly GC-E, also known as RetGC1 or simply GC1, whose activity is tightly controlled by guanylate cyclase-activating proteins (GCAPs) in a Ca^{2+}/Mg^{2+}-dependent manner [2].

GCAP1, encoded by the *GUCA1A* gene, functions as a neuronal Ca^{2+}-sensor belonging to the EF-hand superfamily. The protein harbors four EF-hand motifs (Fig. 1A): EF1 does not bind cations, while EF2, EF3, and EF4 serve as functional Ca^{2+}-binding sites that govern the conformational switch between activating and inhibiting states [3]. Under low Ca^{2+} conditions typical of illuminated photoreceptors, Mg^{2+}-bound GCAP1 adopts an activating conformation that stimulates GC1, promoting cGMP synthesis; conversely, at high Ca^{2+} concentrations characteristic of dark-adapted cells, Ca^{2+}-loaded GCAP1 inhibits the cyclase, preventing excessive nucleotide production [1,2].

The functional GCAP1 pool in photoreceptors comprises dimeric species whose formation is modulated by the cation-bound state [4,5]. Importantly, patients harboring heterozygous *GUCA1A* mutations

* Corresponding author at: Department of Neurosciences, Biomedicine and Movement Sciences, Section of Biological Chemistry, University of Verona, Strada Le Grazie 8, 37134, Verona, Italy.
E-mail address: daniele.dellorco@univr.it (D. Dell'Orco).

https://doi.org/10.1016/j.ijbiomac.2026.151333
Received 6 February 2026; Received in revised form 6 March 2026; Accepted 7 March 2026
Available online 10 March 2026

express both wild-type and mutant proteins, resulting in a heterogeneous mixture of homodimers and heterodimers with potentially distinct regulatory properties [6]. More than twenty missense mutations in *GUCA1A* have been linked to autosomal dominant cone dystrophy (adCOD) and cone-rod dystrophy (adCORD), progressive disorders characterized by central vision loss, colour vision defects, and photophobia (reviewed in [7]). Despite considerable phenotypic variability, a unifying molecular hallmark of these mutations is the constitutive activation of GC1, which disrupts Ca^{2+}/cGMP homeostasis and ultimately triggers photoreceptor degeneration [8]. Disease-associated substitutions predominantly cluster within the Ca^{2+}-coordinating EF-hand motifs, particularly EF3 and EF4, where they impair Ca^{2+} binding, except for a few cases [9], and compromise the inhibitory function of GCAP1.

Among the pathogenic variants, the E111V substitution in EF3 causes a severe CORD phenotype [10]. Replacement of the bidentate Ca^{2+}-coordinating glutamate by valine dramatically reduces Ca^{2+} affinity (~ 80-fold increase in the apparent K_D), shifting the IC_{50} for GC1 inhibition from the physiological range to values effectively outside the Ca^{2+} concentrations experienced by photoreceptors [10]. Molecular dynamics simulations suggested that E111V-GCAP1 exhibits increased backbone flexibility in the EF3/EF4 region when Ca^{2+}-bound, while displaying a more rigid structure in the Mg^{2+}-loaded state [6,10]. The N104H variant, located in the same EF3 loop, similarly impairs Ca^{2+} sensing with doubled IC_{50} values and reduced dynamic range of GC1 regulation [11]. Other mutations affecting the EF3-EF4 region include D100G and E155G, the latter representing the first disease-associated mutation directly eliminating a bidentate Ca^{2+}-coordinating residue [12,13].

Retinal degeneration protein 3 (RD3) has emerged as a crucial regulator of photoreceptor guanylate cyclases. This 23-kDa protein serves dual functions: facilitating GC1 trafficking from the inner segment to the outer segment disk membranes, and acting as a potent allosteric inhibitor of cyclase activity [14,15]. RD3 binds GC1 with nanomolar affinity (IC_{50} ~ 3–5 nM for wild-type) and competitively inhibits GCAP-mediated activation, likely by obstructing the GCAP binding interface or inducing conformational changes in the cyclase dimer [15,16]. The NMR structure of RD3 revealed an elongated four-helix bundle (~ 70 Å × 30 Å; PDB: 6DRF; see Fig. 1B) with the GC1-binding interface localized to a contiguous surface involving helix α3 and adjacent regions [17]. Mutations truncating RD3 at residue 106 or disrupting this interface cause Leber congenital amaurosis type 12 (LCA12), underscoring the protein's essential role in photoreceptor survival [18].

Beyond its interaction with GC1, RD3 has been shown to associate with GCAP1, forming a ternary RD3-GCAP1-GC1 complex that appears essential for proper cyclase trafficking and localization [19]. Direct binding between RD3 and GCAP1 was demonstrated biochemically, suggesting that this interaction may occur post-synthesis in the endoplasmic reticulum [19]. More recently, surface plasmon resonance experiments confirmed that wild-type GCAP1 directly interacts with RD3 with micromolar affinity (K_D = 2.7 μM), while intriguingly, the E111V variant showed no detectable binding [6]. Furthermore, the co-presence of RD3 with an excess of WT-GCAP1 over E111V-GCAP1 restored nearly physiological Ca^{2+}-sensitivity of GC1 regulation, suggesting therapeutic potential for biologics-based approaches [6].

Despite these advances, critical questions remain regarding the molecular determinants governing the GCAP1-RD3 interaction. Specifically, whether this interaction exhibits Ca^{2+}-dependence analogous to the GCAP1-GC1 regulatory mechanism, and how inherited retinal dystrophy (IRD)-associated mutations beyond E111V affect RD3 binding, have not been systematically investigated. In the present study, we address these questions by examining the interaction between RD3 and GCAP1 variants carrying mutations in EF3 (N104H, D100G, E111V) and EF4 (E155G) (see Fig. 1A). Using a combination of NMR spectroscopy, surface plasmon resonance, computational modeling, enzymatic assays,

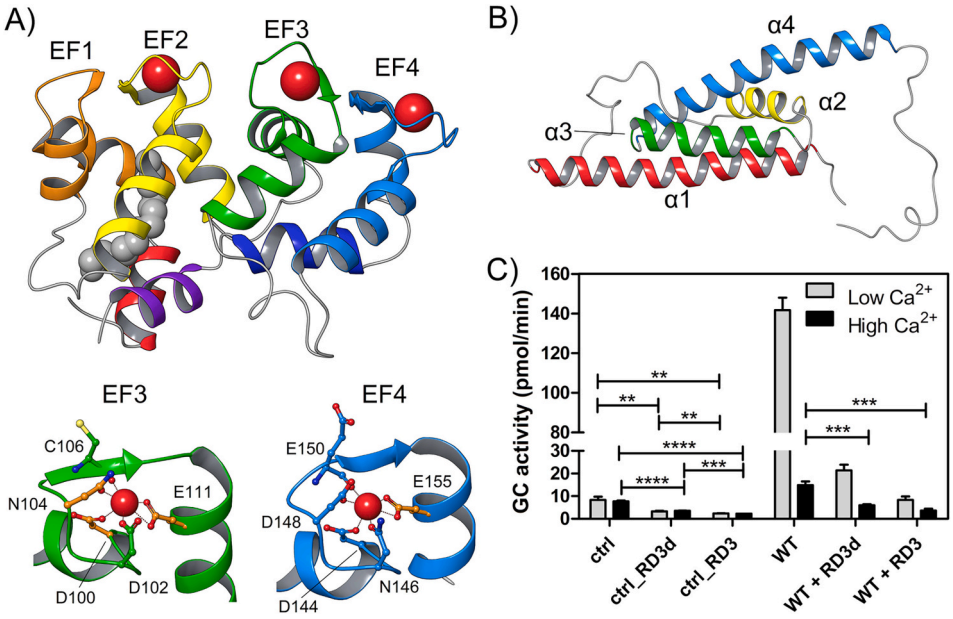

Fig. 1. Three-dimensional structure of GCAP1, RD3 and GC1 enzymatic assays in the presence of RD3d vs RD3. A) The three-dimensional structure of Ca^{2+}-bound human GCAP1 is shown as cartoons with the N-terminal helix in red, EF1 in orange, EF2 in yellow, EF3 in green, EF4 in azure, the transient helix in dark blue and the C-terminal helix in purple. The myristoyl group is shown as grey spheres, Ca^{2+}-ions are represented as red spheres. Insets below display the Ca^{2+}-coordinating residues of EF3 (left, green) and EF4 (right, azure) motifs shown as sticks with C-atoms in green and azure, respectively, while those of IRD-associated residues are represented in orange; N-atoms in dark blue, O-atoms in red and S-atoms in pale yellow. B) The three-dimensional structure of RD3d is shown as cartoon with helix α1 in red, α2 in yellow, α3 in green and α4 in azure. C) Enzymatic GC1 assays performed incubating GC1 with 200 nM RD3 or RD3d in the presence of low (< 19 nM) or high (~ 30 μM) Ca^{2+}, in the absence and in the presence of 5 μM WT-GCAP1. The GC1 activity is shown as pmol of cGMP produced per minute of reaction; data are reported as average ± standard deviation of three technical replicates and the statistical significance of the differences was assessed by two-tailed Student's *t*-test with a threshold of $p < 0.05$. The number of asterisks represents the p-value: ** for $p < 0.01$, *** for $p < 0.001$, **** for $p < 0.0001$.

and immunohistochemistry in murine retinal explants, we demonstrate that the GCAP1-RD3 interaction is Ca^{2+}-dependent and differentially affected by disease-associated mutations. Our findings provide new mechanistic insights into the supramolecular complexes regulating cGMP synthesis in photoreceptors and have implications for understanding the pathophysiology of GCAP1-associated retinal dystrophies.

2. Materials and methods

2.1. Protein expression and purification

2.1.1. RD3

Human RD3 was heterologously expressed in *E. coli* BL21(DE3) after transformation with a pETM-11 plasmid containing RD3 cDNA (Uniprot entry: Q7Z3Z2) provided by Prof. K.-W. Koch (University of Oldenburg), and purified following the protocol detailed in [6,15] with some modifications. Briefly, 1.5 l of LB containing 100 μg/ml Kanamycin were inoculated with a previously prepared glycerol stock stored at −80 °C and incubated at 37 °C and 180 rpm until OD_{600} reached 0.6. Protein expression was induced with 1 mM IPTG for 4 h at 30 °C and then overnight at 4 °C. The following morning cells were harvested by 10 min centrifugation at 5000 × g, then the bacterial pellet was resuspended in cold lysis buffer containing 10 mM Tris-HCl pH 8, 2 mM EDTA, 14 mM β-mercaptoethanol and 100 μM PMSF, sonicated on ice for 15 min (2 s ON - 3 s OFF cycles), and centrifuged for 30 min at 4 °C at 25000 × g to separate soluble and insoluble fractions. The pellet containing the insoluble fraction was then resuspended in the same cold lysis buffer, sonicated for 10 min (2 s ON – 3 s OFF cycles), and centrifuged for 30 min at 4 °C at 25000 × g to remove contaminants. After repeating the washing procedure twice, the insoluble fraction was then resuspended in cold lysis buffer, added with 8 M urea, denatured overnight at 4 °C and renatured by dialysis at 4 °C against 3 × 1 l of 10 mM Tris-HCl pH 7.5, 0.1 mM EDTA and 14 mM β-mercaptoethanol. Finally, refolded RD3 was centrifuged for 30 min at 4 °C at 25000 × g and, after assessing its purity by SDS-PAGE (>90%), stored in 50% glycerol v/v at −80 °C until use.

2.1.2. RD3d

Human RD3d (residues 18–160) was heterologously expressed in *E. coli* BL21(DE3) after transformation with a pET11d plasmid containing RD3d cDNA and purified according to the procedure elucidated in [17] with some modifications. Briefly, 1 l of LB containing 100 μg/ml Ampicillin were inoculated with a previously prepared glycerol stock stored at −80 °C, incubated at 37 °C and 180 rpm until OD_{600} reached 0.6, when protein expression was induced with 1 mM IPTG for 4 h at 37 °C. Cells were harvested by 10 min centrifugation at 5000 × g, then the bacterial pellet was resuspended in cold lysis buffer containing 10 mM Tris-HCl pH 8, 2 mM EDTA, 14 mM β-mercaptoethanol and 100 μM PMSF, sonicated on ice for 15 min (2 s ON – 3 s OFF cycles), and centrifuged for 30 min at 4 °C at 25000 × g to separate soluble and insoluble fractions. The pellet containing the insoluble fraction was then resuspended in the same cold lysis buffer, added with 8 M urea, denatured overnight at 4 °C and renatured by dialysis at 4 °C against 3 × 1 l of 10 mM Tris-HCl pH 8, 0.1 mM EDTA and 14 mM β-mercaptoethanol. Refolded RD3d was then purified via Hydrophobic Interaction Chromatography using a phenyl-sepharose (HIC, HiLoad 26/10 Phenyl Sepharose® High Performance, GE Healthcare) column previously equilibrated with 20 mM Tris-HCl pH 8, 1 mM DTT and 1 M NaCl. Protein was then loaded and eluted using 20 mM Tris-HCl pH 8, 1 mM DTT; fractions containing RD3d were further purified via Anionic Exchange Chromatography (AEC, HiPrep Q HP 16/10, GE Healthcare) using the same buffer and a 0 to 1 M NaCl gradient in 100 ml followed by a final Size Exclusion Chromatography (SEC, HiPrep 26/60 Sephacryl S-200 HR, GE Healthcare) step in 20 mM Tris pH 8, 100 mM NaCl, 1 mM DTT. The purest fractions were flash-frozen with liquid nitrogen and stored at −80 °C until use.

2.1.3. GCAP1 variants

WT-GCAP1 was heterologously expressed in *E. coli* after transformation with pET-11a containing the cDNA of human WT-GCAP1 (Uniprot entry: P43080) purchased from Genscript with the E6S variant for the consensus sequence for N-terminal myristoylation. The E111V variant was introduced using QuikChange II Site-Directed Mutagenesis kit (Agilent) as detailed in [10], while plasmids containing the cDNA of D100G, N104H and E155G variants were purchased by Genscript as mutagenesis service on the WT-GCAP1 plasmid. GCAP1 variants were heterologously expressed in *E. coli* BL21(DE3) after co-transformation with pBB131 vector encoding for *S. cerevisiae* N-myristoyltransferase (yNMT) required for post-translational myristoylation of the N-terminal Gly [20] and purified using the same protocol as previously detailed [10]. Briefly, 1 l of LB containing 100 μg/ml Ampicillin and 30 μg/ml Kanamycin were inoculated with a previously prepared glycerol stock stored at −80 °C, incubated at 37 °C and 180 rpm until OD_{600} reached 0.4, when 50 μg/ml myristic acid in 50% EtOH was added to the medium. At OD_{600} = 0.6 protein expression was induced with 1 mM IPTG for 4 h at 37 °C, then cells were harvested by 10 min centrifugation at 5000 × g and the bacterial pellet was lysed for 1 h at 37 °C in 20 mM Tris-HCl pH 7.5, 150 mM NaCl, 5 U/ml DNAse I, 100 μg/ml lysozyme, 14 mM β-mercaptoethanol and protease inhibitor cocktail before 30 min centrifugation at 4 °C at 25000 × g to separate soluble and insoluble fractions. Insoluble GCAP1 variants were extracted from inclusion bodies after denaturation with 6 M guanidine-HCl and refolding via dialysis against 20 mM Tris-HCl pH 7.5, 150 mM NaCl, 14 mM β-mercaptoethanol buffer. Proteins were purified via a combination of Size Exclusion Chromatography (SEC, HiPrep 26/60 Sephacryl S-200 HR, GE Healthcare) in 20 mM Tris-HCl pH 7.5, 150 mM NaCl, 14 mM β-mercaptoethanol buffer and Anionic Exchange Chromatography (AEC, HiPrep Q HP 16/10, GE Healthcare) in 20 mM Tris-HCl pH 7.5, 14 mM β-mercaptoethanol buffer using a linear gradient from 0 to 1 M NaCl in 200 ml. GCAP1 variants concentration was measured by Bradford assay [21] using a GCAP1-specific calibration curve based on quantification of the amino acid content (Alphalyze), and their purity verified on a 15% SDS-PAGE gel. Finally, GCAP1 variants were exchanged against 50 mM NH_4HCO_3 buffer, flash-frozen in liquid nitrogen, lyophilized and stored at −80 °C until use.

2.2. Guanylate cyclase assays

The effect of RD3 and RD3d on the GCAP1 variants-mediated regulation of Guanylate Cyclase 1 (GC1) activity was investigated by performing enzymatic assays and by monitoring cGMP synthesis following the procedure detailed in [22]. Briefly, human recombinant GC1 was expressed stably in HEK293 cells after transfection with pcDNA3.1 + N-eGFP containing the cDNA of human GC1 and resulting in a fusion protein constituted by eGFP at the N-terminal and GC1 as previously described [22]. GC1 was isolated from HEK293 membranes after cell lysis and centrifugation, and resuspended in 50 mM HEPES pH 7.4, 50 mM KCl, 20 mM NaCl and 1 mM DTT.

The effects of RD3 and RD3d on the WT-GCAP1-mediated minimal and maximal activation of GC1 were determined by incubating at room temperature for 5 min 5 μM WT-GCAP1 with 200 nM RD3 or RD3d and GC1, in the presence of low (< 19 nM) or high (~ 30 μM) Ca^{2+}. After addition of reaction buffer (75 mM MOPS pH 7.2, 150 mM KCl, 10 mM NaCl, 2.5 mM DTT, 8.75 mM $MgCl_2$, 2.5 mM GTP, 0.75 mM ATP, 0.4 mM Zaprinast), samples were incubated for 5 min at 30 °C, finally the reaction was stopped by adding 75 mM EDTA and heating the samples at 96 °C for 5 min.

The effects of GCAP1 variants (WT, D100G, N104H, E111V and E155G) on the regulation of GC1 in the presence of RD3d were investigated by performing the same assay as described above with 200 nM RD3d and 5 μM GCAP1 variants.

After stopping the reaction, samples were centrifuged for 30 min at 4 °C at 20000 × g, the supernatant collected and injected into an HPLC

system using a reversed-phase C18 column (LiChrosphere 100 RP-18, Merck). cGMP was separated using a methanol gradient, identified by its characteristic retention time and quantified by peak area integration and comparison with a cGMP-specific calibration curve. Data is reported as mean ± standard deviation of three technical replicates and the statistical significance of the observed differences was assessed by two-tailed Student's *t*-test with significance threshold set at $p < 0.05$ (indicated by asterisks in Fig. 1C and Fig. 6). Due to the impossibility to precisely quantify GC1 over the total amount of membrane proteins, the total amount of cGMP synthesized per minute of reaction is dependent on the membrane batch used for the experiment. The results reported in Fig. 1 and Fig. 6 were collected using different membrane batches, thus WT-GCAP1 was used as an internal standard to which all other conditions were compared.

2.3. Nuclear magnetic resonance

NMR experiments were performed on uniformly ^{15}N-labeled RD3d in the presence of unlabeled myristoylated WT-GCAP1 or E111V-GCAP1. The ^{15}N-labeled RD3d protein was prepared as described previously [17]. NMR samples consisted of ^{15}N-labeled RD3d (0.18 mM) and unlabeled GCAP1 (0.3 mM) dissolved in 10 mM Tris-d_{11}, 2 mM dithiothreitol-d_{10}, 8% D_2O at pH 7.4. Samples containing either Ca^{2+}-bound or Mg^{2+}-bound GCAP1 were generated by adding 2 mM $CaCl_2$ or 2 mM $MgCl_2$, respectively. All NMR experiments were recorded at 25 °C using a Bruker 800 MHz Avance III NMR spectrometer equipped with a triple-resonance cryogenic TCI probe and pulsed field gradients. Two-dimensional ^{15}N—^{1}H HSQC experiments were acquired using 2048 (^{1}H) x 256 (^{15}N) data points, ^{1}H sweep width of 10,000 Hz, and ^{15}N sweep width of 2430 Hz. The NMR data were processed using NMRPipe [23].

2.4. Surface plasmon resonance

Surface plasmon resonance (SPR) measurements were conducted using a SensiQ Pioneer system equipped with a COOH1 sensor chip (Sartorius), following the procedure detailed in [6]. The chip was preconditioned by performing two cycles of sequential injections of 25 μl HCl 0.1 M, 25 μl NaOH 50 mM, 25 μl SDS 0.5%, and 25 μl EDTA 0.3 M at 100 μl/min flowrate, according to the manufacturer protocol.

RD3 and RD3d were covalently immobilized on the sensor chip surface through site-specific thiol-disulfide exchange chemistry. Briefly, the chip surface was activated upon 70 μl injection of a 50 mM N-hydroxysuccinimide (NHS) and 200 mM N-ethyl-N′-(dimethylaminopropyl)-carbodiimide (EDC) solution at 5 μl/min, followed by 70 μl injection of 80 mM 2-(2-pyridinyldithio)ethaneamine hydrochloride (PDEA) dissolved in in 0.1 M sodium borate buffer (pH 8.5), at 5 μl/min. RD3 and RD3d were then exchanged against bi-distilled water using PD10 desalting coulmns (Cytiva), quantified (by absorption at 280 nm using extinction coefficients $\varepsilon = 32{,}092\ M^{-1}\ cm^{-1}$ and $\varepsilon = 21{,}000\ M^{-1}\ cm^{-1}$ -estimated from the sequences by Expasy- respectively), and immobilized on the chip surface resulting in 792 RU and 930 RU, respectively. Finally, residual reactive thiol groups were inactivated by a 50 μl injection of 70 mM L-cysteine and 1 M NaCl dissolved in 10 mM sodium acetate buffer (pH 4) at 5 μl/min.

Binding kinetics between RD3d and GCAP1 variants were assessed by injecting 200 μl of GCAP1 variants at 0.5, 1 and 2 μM concentration at 20 μl/min and monitoring association and dissociation for 600 s. GCAP1 variants were resuspended in 10 mM HEPES, 150 mM NaCl, 0.005% Tween-20, pH 7.4 (supplemented with either 0.5 mM EGTA and 1 mM Mg^{2+} or 1 mM Mg^{2+} and 0.3 mM Ca^{2+}), quantified via Bradford assay by comparing the absorbance with a GCAP1-specific calibration curve (Alphalyze) to achieve the desired concentrations for the assay, and injected in alternated fashion (3 injections of WT followed by 3 injections of each mutant) to minimize potential artifacts due to chip ageing. Three cycles of injections were performed for each variant, resulting in 9 injections per variant. When possible, the dissociation rate constant was estimated by fitting the dissociation phase of the sensorgram to a first-order exponential decay model:

$$RU(t) = RU_0 \cdot e^{-k^{off} \cdot t} \tag{3}$$

where RU_0 is the maximum response at each analyte (GCAP1 variant) concentration and k^{off} is the dissociation rate constant, which was calculated for WT-GCAP1 in the co-presence of Mg^{2+} and Ca^{2+} and reported as average ± standard error of the mean of 9 injections.

The association phase was fitted to the following pseudo-first order equation:

$$RU(t) = \frac{k^{on} \cdot R_{max} \cdot [GCAP1]}{k^{on} \cdot [GCAP1] + k^{off}} \left(1 - e^{-\left(k^{on} \cdot [GCAP1] + k^{off}\right) \cdot t}\right) + R_0 \tag{4}$$

where R_0 is the baseline, R_{max} is the theoretical maximum SPR response assuming complete occupancy of RD3 binding sites, and [GCAP1] is the GCAP1 variant concentration at each injection. Finally, the association rate constant k^{on} was estimated as average ± standard error of the mean of 9 injections, allowing for the estimation of the equilibrium dissociation constant K_D based on the ratio between dissociation and association rate constants ($K_D = k^{off}/k^{on}$).

2.5. Molecular modeling of the GCAP1-RD3 complex with AlphaFold 3

The three-dimensional structure of the GCAP1-RD3 complex was predicted using the server version (https://alphafoldserver.com/) of AlphaFold3 [24] after providing the sequences of human GCAP1 (Uniprot: P43080) and human RD3 (Uniprot: Q7Z3Z2) as input. As GCAP1 undergoes a post-translational modification which is not available on the web server, namely myristoylation of the N-terminal Gly, myristic acid was included as ligand. Moreover, since RD3 was demonstrated to specifically interact with Ca^{2+}-bound GCAP1, three Ca^{2+}-ions were also included in the input. The AlphaFold3 server automatically generated five structural models of the complex and the respective scoring values integrating i) predicted local distance difference test (pLDDT) scores, ii) predicted aligned error (PAE) metrics, iii) predicted template modeling (pTM) score and iv) the interface predicted template modeling (ipTM). Model selection was achieved after visual inspection with Maestro BioLuminate (Schroedinger), identification of the interface and filtering according to the presence of residues presenting differences in chemical shifts from NMR experiments (see results). To overcome the limitation of the missing post-translational myristoylation and to prevent potential artifacts due to the missing covalent bond with the N-terminal Gly, the structure of GCAP1 obtained by homology modeling and previously employed to predict GCAP1 dimerization [6] was superimposed to the selected model. Cα-RMSD calculated on EF1 and EF1-EF2 motifs (residues 14–42 and 14–82, respectively) showed satisfactory agreement between the models, with values below 1.09 Å, and finally, the so-obtained hybrid model was minimized with Maestro BioLuminate (Schroedinger), using OPLS4 forcefield (Schroedinger, New York, NY) and 0.3 Å as threshold for the Root-Mean Square Displacement (RMSD) of heavy atoms.

2.6. Immunohistochemistry of mouse retinas

Animal experiments were approved by the Animal Care and Use Committee (CIRSAL) of the University of Verona and authorized by the Italian Ministry of Health, in full compliance with the European Communities Council Directive 2010/63/EU and ARRIVE guidelines. Mice were housed under standardized conditions with controlled temperature and humidity, a 12-h light/dark cycle, and ad libitum access to food and water. Both male ($n = 2$) and female (n = 2) mice were used in this study, as the pathology under investigation is not sex related.

Wild-type C57BL/6J mice ($n = 4$) were anesthetized with isoflurane

and euthanized via cervical dislocation at 30 postnatal days (p30). After enucleation, the eyes were punctured and submerged in 10% neutral buffered formalin (NBF) overnight at 4 °C. The following day, the corneas and lenses were microdissected, and the remaining eyecups were fixed for an additional 2 h at room temperature (RT). Tissues were then dehydrated through 15 min incubation with a graded ethanol series (70%–100% v/v) at RT, with a final overnight incubation in 100% ethanol at 4 °C. After clearing in xylene for 2 h, samples were embedded in paraffin and sectioned at 7 μm by microtome. Sections were mounted on poly-L-lysine-coated slides and dried overnight at 37 °C. For immunohistochemical analysis, sections were deparaffinized in xylene and rehydrated through a descending ethanol gradient (100% to 70% v/v). Antigen retrieval was performed in citrate buffer (pH 6.0) at 85 °C for 20 min, followed by a 1-h incubation in blocking solution (20% Normal Goat Serum and 0.5% Tween-20 in PBS). Primary antibodies were diluted in 0.5% BSA/PBS and incubated in a humidified chamber overnight at 4 °C. The following antibodies were used: anti-GC1 (Novus Biologicals, NBP3-12211), anti-RD3 (Invitrogen, PA5-83117) and anti-GCAP1 (Novus Biologicals, NBP3-17717). Secondary antibody incubation and detection were carried out using the Leica BOND-III fully automated IHC/ISH system with the BOND-PRIME Polymer AP Detection kit. Sections were counterstained with hematoxylin, and high-resolution images were acquired using an Evident APEX microscope equipped with a 20× objective.

3. Results

Previous studies by some of us demonstrated that full-length RD3 (RD3) inhibits GC1 with an EC_{50} in the nanomolar range [6,17], and that it interacts with Ca^{2+}-bound WT-GCAP1, but not with its IRD-associated variant E111V [6]. Notably, the apparent affinity and inhibitory potency of RD3 toward GC1 vary depending on specific experimental conditions, with reported EC_{50} values ranging from ~ 3 nM to ~ 68 nM [6,15,17], yet consistently remaining within the low nanomolar range. However, it must be noted that RD3 has a distinct tendency to aggregate [15,16], which limits the number of in vitro techniques applicable to this system due to the high concentration required. To overcome this limitation, a truncated form of RD3 encompassing residues 18–160 (RD3d), thus missing both N- and C-terminal stretches was engineered [17], resulting in increased solubility and monomeric structure even at concentrations as high as 300 μM, which are often required for high-resolution structural techniques such as solution NMR. We therefore compared the regulation of GC1 by RD3 and RD3d in terms of minimal and maximal cGMP synthesis to exclude potential artifacts arising from the missing regions in RD3d.

3.1. RD3d is functional but less effective than full length RD3

In the presence of RD3d, and even more so of RD3, GC1 catalytic activity under both light- and dark-mimicking Ca^{2+} concentrations (<19 nM and 30 μM, respectively) was significantly lower than basal activity (Fig. 1C), in line with previous results [17]. Moreover, these results confirmed that GC1 inhibition by RD3 is cation-independent, does not require the presence of GCAP1, and that the deleted N- and C-terminal regions are not essential for GC1 inhibition [17]. A similar behavior could be observed when the physiological Ca^{2+}-dependent GC1 regulator WT-GCAP1 was also present, as cGMP synthesis was significantly decreased in the presence of both RD3d and RD3 at both low (activating) and high (inhibiting) Ca^{2+} concentrations.

The X-fold, representing the Ca^{2+}-dependent increase in cGMP synthesis with respect to that under inhibiting GC1 conditions ($(GC1^{low\_Ca2+}\text{-}GC^{high\_Ca2+})/GC^{high\_Ca2+}$), allowed us to quantify such effect, highlighting a decrease from 8.6 ± 1.2 in the absence of RD3 variants to 2.6 ± 0.2 and 1.4 ± 0.8 in the presence of RD3d and RD3, respectively (Fig. 1C).

Overall, these results confirmed that RD3d is functional and recapitulates the biological function of RD3, albeit with lower efficiency, hence, due to its higher solubility, all subsequent experiments were performed using RD3d.

3.2. Insights into RD3d-GCAP1 interaction by nuclear magnetic resonance

Full-length RD3 was found to interact with Ca^{2+}-bound GCAP1, but not with the IRD-associated variant E111V [6]; however, no information was available regarding the interaction of RD3 with Mg^{2+}-bound GCAP1. Mg^{2+} is abundant in photoreceptor outer segments, and its concentration (~ 1 mM) remains essentially constant upon cell illumination, suggesting it does not participate in the dynamic regulation of phototransduction [25]. Nevertheless, Mg^{2+} binds GCAP1 and modulates its regulatory properties toward GC1 [2,26], making it relevant to assess its potential influence on the GCAP1-RD3 interaction. To probe atomic-level interactions between RD3d and GCAP1, we performed NMR experiments on isotopically labeled RD3d in the presence of saturating Mg^{2+}-bound vs Ca^{2+}-bound GCAP1. The RD3d construct (residues 18–160) was used for all NMR studies because of its higher solubility compared to full-length RD3 [17], which provided submillimolar concentrations of RD3d required for high-resolution structural studies. NMR spectra of RD3d confirmed that it interacts with both Ca^{2+}-bound and Mg^{2+}-bound WT-GCAP1 (Fig. 2).

Two-dimensional $^{1}H—^{15}N$ HSQC spectra of ^{15}N-labeled RD3d alone as a negative control (black peaks, Fig. 2A) and in the presence of saturating and unlabeled Mg^{2+}-bound WT-GCAP1 (red peaks, Fig. 2A) revealed that the chemical shift of most NMR peaks remained unchanged. However, eight peaks exhibited detectable chemical shift changes that were assigned to RD3d residues: V71, S91, Q107, E110, V111, V114, Q116 and L117. These peaks represent exposed residues in the NMR structure of RD3d (Ref. [17]), which suggests these residues might contact Mg^{2+}-GCAP1.

Fig. 2B shows a two-dimensional $^{1}H—^{15}N$ HSQC spectrum of ^{15}N-labeled RD3d in the presence of saturating and unlabeled Ca^{2+}-bound WT-GCAP1 (Fig. 2B, red peaks) overlaid on the spectrum of ^{15}N-labeled RD3d alone (Fig. 2B, black peaks). The circled peaks in Fig. 2B (assigned to G94 and unassigned amide side chain) become broadened beyond detection in the presence of Ca^{2+}-bound WT-GCAP1. The peak broadening is consistent with GCAP1 binding to RD3d as seen by SPR [6]. However, the majority of NMR peaks were not broadened and did not exhibit any chemical shift change upon the addition of GCAP1. The relatively small overall spectral change here suggests that Ca^{2+}-bound WT-GCAP1 binding to RD3d may not cause a large structural change in RD3d. The NMR peaks with the largest spectral change were assigned to RD3 residues: S20, E23, M24, L29, I88, H89, C93, G94, and L98 (Fig. 2B). These residues are solvent-exposed in RD3d and map to a localized region on the surface of the NMR structure of RD3d [17].

Fig. 2C shows a two-dimensional $^{1}H—^{15}N$ HSQC NMR spectrum of ^{15}N-labeled RD3d in the presence of unlabeled Mg^{2+}-$GCAP1^{E111V}$ (Fig. 2C, red peaks) overlaid on the spectrum of ^{15}N-labeled RD3d alone (Fig. 2C, black peaks). Fig. 2D shows a similar NMR spectrum of ^{15}N-labeled RD3d in the presence of unlabeled Ca^{2+}-$GCAP1^{E111V}$ (Fig. 2D, red peaks) overlaid on the spectrum of RD3d alone (Fig. 2D, black peaks). The spectra reveal that the addition of either Mg^{2+}-$GCAP1^{E111V}$ or Ca^{2+}-$GCAP1^{E111V}$ to RD3d did not cause any detectable NMR spectral change. These results suggest that both Mg^{2+}-bound and Ca^{2+}-bound forms of GCAP1 with the E111V mutation do not bind to RD3d, consistent with the IRD-associated GCAP1 variant abolishing the interaction with RD3d, as seen by prior surface plasmon resonance experiments performed on the full-length protein [6].

3.3. Surface plasmon resonance highlights the role of Ca^{2+} in GCAP1-RD3d recognition

To investigate the effects of Ca^{2+} and Mg^{2+} on the affinity of the

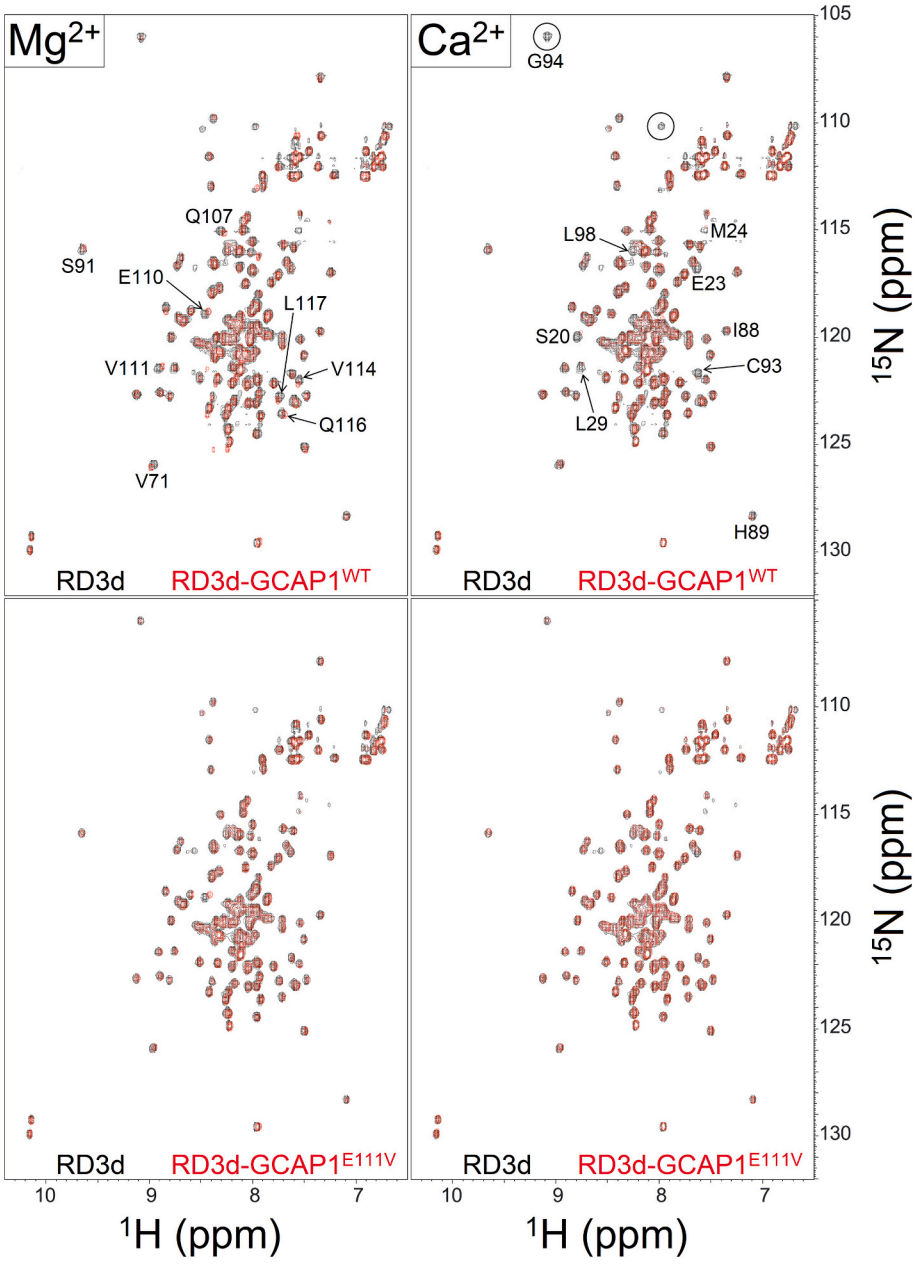

Fig. 2. NMR Spectra of ^{15}N-labeled RD3d in the presence of GCAP1^{WT} vs GCAP1^{E111V}. Top panels: ^{1}H—^{15}N HSQC spectrum of RD3d in the presence of (left) Mg^{2+}-bound GCAP1^{WT} or (right) Ca^{2+}-bound GCAP1^{WT} (red peaks) overlaid on the spectrum of RD3d alone (black peaks). Bottom panels: ^{1}H—^{15}N HSQC spectrum of RD3d in the presence of (left) Mg^{2+}-bound GCAP1^{E111V} or (right) Ca^{2+}-bound GCAP1^{E111V} (red peaks) overlaid on the spectrum of RD3d alone (black peaks). Peaks showing the largest chemical shift difference are highlighted by residue labels. Circled peaks are broadened beyond detection in the presence of GCAP1.

GCAP1-RD3d complex, we injected different concentrations of GCAP1 variants on RD3d (previously site-specifically immobilized on the sensor chip by thiol-disulfide exchange) and monitored the binding process by surface plasmon resonance.

The sensorgrams obtained for WT-GCAP1 showed that, although a slight hint of binding was present even in the presence of Mg^{2+}, Ca^{2+} greatly enhanced the interaction process (Fig. 3A). Only in the presence of Ca^{2+} could the WT-GCAP1:RD3d binding kinetics be adequately described by a 1:1 Langmuir model, yielding an association rate constant $k^{on} = (2.4 \pm 1.2) \times 10^{3}$ M^{-1} s^{-1} (Table 1) and a dissociation rate constant $k^{off} = (3.9 \pm 0.6) \times 10^{-3}$ s^{-1} (Table 1), collectively resulting in a K_D of 1.6 ± 0.8 μM. The estimated K_D of WT-GCAP1 for RD3d was in line with that previously exhibited by full length RD3 (2.7 ± 0.9 μM [6]) under the same experimental conditions, suggesting a negligible role of both the N- and the C-terminus of RD3 in GCAP1 recognition process.

As for IRD-associated GCAP1 variants, SPR experiments on E111V-GCAP1 confirmed NMR results, thus demonstrating that this variant cannot bind RD3d under both GC1-activating and inhibiting conditions (Fig. 3B), similarly to what was previously observed with RD3 [6]. We thus focused only on the investigation of binding kinetics between GCAP1 variants and immobilized RD3d in the presence of Ca^{2+}. Indeed, upon injecting different concentrations of IRD-associated GCAP1 variants, D100G-, N104H-, and E155G-GCAP1 showed 1:1 Langmuir binding (Fig. 4) with similar k^{off} values ranging between $(3.1 \pm 0.2) \times 10^{-3}$ and $(4.1 \pm 0.5) \times 10^{-3}$ s^{-1} for all tested variants (Table 1). Moreover, no major differences could be detected on the association process, as k^{on} exhibited virtually identical values among WT, N104H and D100G variants, spanning between $(2.4 \pm 1.2) \times 10^{3}$ and $(2.7 \pm 1.1) \times 10^{3}$ M^{-1} s^{-1} (Table 1). Overall, the comparable association and dissociation rate constants measured for the variants resulted in similar values for the

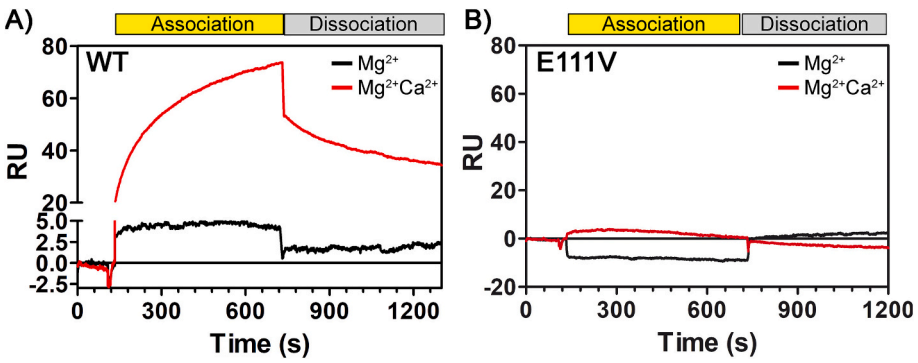

Fig. 3. Ca^{2+}-dependent interaction between RD3d and GCAP1 variants investigated by SPR. Representative sensorgrams obtained injecting 2 μM WT- (A) or E111V-GCAP1 (B) on immobilized RD3d in the presence of 0.5 mM EGTA and 1 mM Mg^{2+} (black lines) or in the presence of 1 mM Mg^{2+} and 300 μM Ca^{2+} (red lines). Complex association and dissociation were followed for 10 min each, setting the flow rate at 20 μl/min and using 10 mM HEPES pH 7.4, 150 mM KCl, 0.005% Tween-20 as running buffer.

Table 1
Kinetic parameters from SPR experiments.

	WT	N104H	D100G	E155G
k^{off} (s^{-1})[a]	$(3.9 \pm 0.6) \times 10^{-3}$	$(4.1 \pm 0.5) \times 10^{-3}$	$(3.1 \pm 0.2) \times 10^{-3}$	$(3.3 \pm 0.6) \times 10^{-3}$
k^{on} (M^{-1} s^{-1})[a]	$(2.4 \pm 1.2) \times 10^{3}$	$(6.5 \pm 2.5) \times 10^{3}$	$(2.7 \pm 1.1) \times 10^{3}$	$(7.4 \pm 3.5) \times 10^{3}$
K_D (M)[b]	$(1.6 \pm 0.8) \times 10^{-6}$	$(0.6 \pm 0.3) \times 10^{-6}$	$(1.1 \pm 0.4) \times 10^{-6}$	$(0.5 \pm 0.2) \times 10^{-6}$

[a] Data are reported as average ± standard error of the mean.
[b] Data are reported as average ± error propagation.

affinity, as shown by K_D values ranging between 1.1 ± 0.4 and 1.6 ± 0.8 μM (Table 1).

Interestingly, E155G-GCAP1, the only IRD-associated variant in this study located in the EF4 motif, showed a 3-fold increase in k^{on} compared to WT [$(7.4 \pm 3.5) \times 10^3$ vs $(2.4 \pm 1.2) \times 10^3$ M^{-1} s^{-1}], ultimately resulting in a 2.8-fold increase in affinity (K_D = 450 ± 230 nM). An allosteric mechanism connecting EF4 with the N-terminal domain, and specifically with EF1, EF2, and the region at the interface with the myristoyl moiety, has been proposed by exhaustive molecular dynamics simulations [27] and confirmed by further experimental studies [28]. The E155G mutation might therefore induce conformational changes in the EF4 region, which are transmitted to the N-terminal domain. The observed effect on k^{on} suggests either that the EF4 region of GCAP1 is critically positioned at the initial recognition interface with RD3d, or that the perturbation induced by the substitution propagates through long-range allosteric effects that favorably affect the association process.

3.4. A structural model for RD3-GCAP1 interaction

Based on the information provided by NMR experiments as to the residues exhibiting chemical shift variations upon RD3d binding in the presence of Ca^{2+}, we performed rigid body docking simulations with either ZDOCK [29] or PIPER [30] on all 10 conformers of RD3d deposited on the PDB (entry: 6DRF), adopting an approach similar to that previously used by some of us to propose a model for GCAP1 dimerization [5]. However, neither algorithm allowed us to identify a complex fulfilling all structural constraints derived from NMR, which required residues S20, E23, M24, L29, I88, H89, C93, G94 and G148 to be located at the RD3d-GCAP1 interface, based on their chemical shift perturbations. Indeed, the N-terminal flexible loop of RD3d was always the only interface of the predicted complexes (results not shown), thus implying that the RD3d interaction interface would form only upon a conformational change, hence that the rigid body assumption made for docking simulations may not be correct. Alternatively, the lack of convergence using the NMR restraints might indicate that some or all of the NMR spectral changes are caused by remote or secondary effects, and perhaps could explain why some of these residues do not contact GCAP1.

We therefore predicted the heterodimeric complex using the AlphaFold3 server [24] after providing the sequences of RD3 and GCAP1 and setting 3 Ca^{2+} ions as ligands to mimic Ca^{2+}-bound GCAP1. It is worth noting that AlphaFold3 has some intrinsic methodological limitations, especially when dealing with proteins undergoing post-translational modifications, such as the N-terminal myristoylation of GCAP1. Indeed, although some post-translational modifications can be now modeled in AlphaFold3 predictions, it was not possible to covalently link a myristoyl group to the GCAP1 N-terminal Gly residue. Instead, myristic acid was set as a ligand bound non-covalently to GCAP1 in order to mimic the myristoylated, physiologically relevant form of GCAP1.

The analysis of the 5 complexes modeled by AlphaFold3 highlighted that the first two models had higher pTM, representing the global quality of the fold, compared to models 3, 4, and 5 (0.37 vs 0.35, Table 2), while the quality of the interface (ipTM) was found to be higher for models 2 and 3 compared to models 1, 4 and 5 (0.15 vs 0.14, Table 2). These metrics concur with the calculation of the ranking score of the 5 models, which was identical for the first 3 models (0.31, Table 2) and higher than the scores for model 4 (0.30, Table 2) and 5 (0.29, Table 2), indicating that the three models proposed were equally reasonable, at least from a prediction standpoint. Interestingly though, none of the residues displaying chemical shift differences upon interacting with Ca^{2+}-bound GCAP1 were located on the predicted interface of models 1 and 2, while residues M24, C93 and G94 were identified as interfacial residues for models 3, 4 and 5, thus suggesting that model 3 may be the most reliable RD3-GCAP1 complex both in terms of quality of prediction and adherence to NMR data. However, as the N-terminal region of GCAP1 was modeled without the post-translational modification but with the myristic acid as a ligand, we calculated the Cα-RMSD of the EF1 motif (residues 14–42) and of both EF1 and EF2 motifs (residues 14–82) with respect to the structure of human GCAP1 representing the centroid of 4 μs molecular dynamics simulations and previously used to predict GCAP1 dimerization [6]. Since model 3 (Fig. 5) exhibited satisfactory agreement with the homology model for EF1 (Cα-RMSD = 0.83 Å) as well as for EF1-EF2 (Cα-RMSD = 1.09 Å), the GCAP1 molecule in the

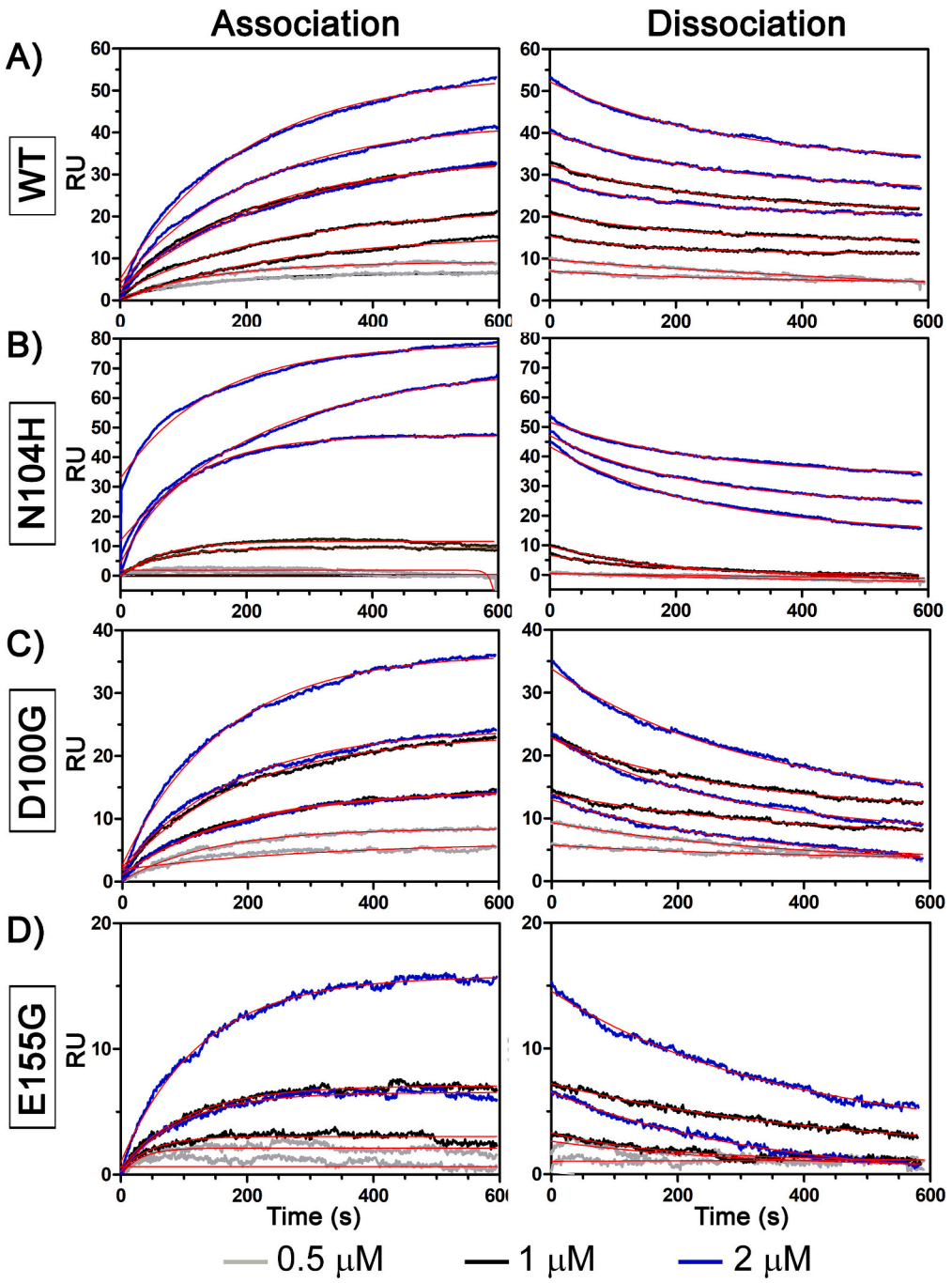

Fig. 4. Effects of IRD-associated mutations on the kinetics of the interaction between RD3d and GCAP1. Sensorgrams collected injecting 0.5 μM (grey lines), 1 μM (black lines) and 2 μM (blue lines) of GCAP1 variants A) WT, B) N104H, C) D100G, and D) E155G on immobilized RD3d. Complex association and dissociation were followed for 10 min each, setting the flow rate at 20 μl/min and using 10 mM HEPES pH 7.4, 150 mM KCl, 0.005% Tween-20, 1 mM Mg^{2+} and 300 μM Ca^{2+} as running buffer. Red lines represent the fitting curve according to a Langmuir 1:1 model.

Table 2
Evaluation of the predictions of the RD3d-GCAP1 complex by Alphafold 3, [a] global fold quality, [b] interface quality.

Model	pTM[a]	ipTM[b]	Ranking score
1	0.37	0.14	0.31
2	0.37	0.15	0.31
3	0.35	0.15	0.31
4	0.35	0.14	0.30
5	0.35	0.14	0.29

complex predicted by AlphaFold3 was replaced by that obtained by homology modeling to avoid structural artifacts due to AlphaFold3 treating the N-terminal covalently bound myristoyl group as a ligand. Based on both the quality metrics and consistency with NMR data, Model 3 was therefore selected as the most realistic representation of the GCAP1-RD3 complex.

The structural analysis of the GCAP1-RD3 complex highlighted a rather extended interface (Fig. 5A) constituted mainly by the N-terminal region (not present in our NMR experiments) of RD3, the C-terminal part of helix α2, the loop connecting α2 and α3, and the N-terminal part of helix α3, together with the exiting helix of the EF1 motif of GCAP1, the

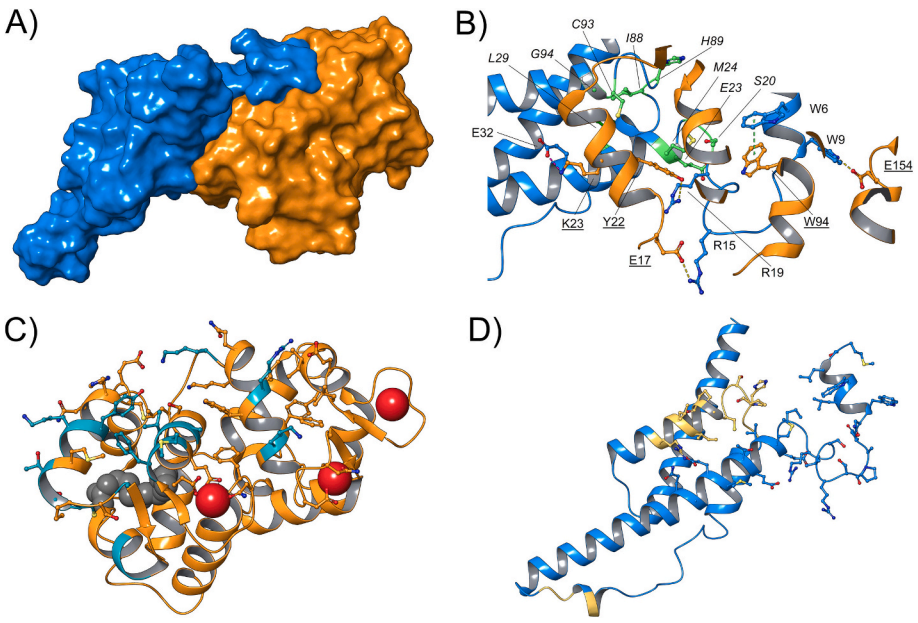

Fig. 5. Structural details of the GCAP1-RD3 complex predicted by AlphaFold3. A) Relative orientation of GCAP1 and RD3 as predicted by AlphaFold3 compatible with NMR-derived constraints and optimized as described in methods section. Proteins are represented as surface with GCAP1 in orange and RD3 in azure. B) Structural details of the GCAP1-RD3 binding interface. The three-dimensional structure of the GCAP1-RD3 complex is shown as cartoon with RD3 in azure and GCAP1 in orange. H-bonds, salt bridges and π-π interactions are shown as yellow, purple and green dashed lines, respectively, residues involved in such interactions are shown as sticks (residues involved in van der Waals interactions are not shown for clarity), with C-atoms colored azure (RD3) and orange (GCAP1), O-atoms in red, N-atoms in dark blue and S-atoms in yellow and labeled, with GCAP1 residues underlined. RD3 residues exhibiting chemical shift differences upon interaction with GCAP1 are shown in green and labeled in italics. C) The three-dimensional structure of GCAP1 is shown as orange cartoon with Ca^{2+}-ions and the myristoyl group represented as red and grey spheres, respectively. Residues belonging to the interface with RD3 are represented as sticks with C-atoms colored orange, O-atoms in red, N-atoms in dark blue and S-atoms in yellow. Residues involved in GC1 binding [31–33] are colored teal. D) The three-dimensional structure of RD3 is shown as azure cartoon, residues belonging to the interface with GCAP1 are represented as sticks with C-atoms colored azure, O-atoms in red, N-atoms in dark blue and S-atoms in yellow. Residues involved in GC1 regulation [16,17,34] are colored yellow.

entering helices of EF2 and EF3 motifs and the Ca^{2+}-binding loop of EF4. Moreover, although the interaction between GCAP1 and RD3 appeared mainly driven by van der Waals interactions, as shown by their shape complementarity (Fig. 5A), it is stabilized by H-bonds between RD3-W9 and GCAP1-E154, RD3-R15 and GCAP1-E17, RD3-R19 and GCAP1-Y22, by a salt bridge between RD3-E32 and GCAP1-K23, and by a π-π interaction between RD3-W6 and GCAP1-W94 (Fig. 5B). Interestingly, the RD3-GCAP1 interface seems to be partially overlapped to both GCAP1-GC1 [31–33] (Fig. 5C), and GC1-RD3 [16,17,34] interfaces, although it must be noted that the second RD3-GC1 binding interface, which lies at the beginning of the loop connecting helices α1 and α2 (residues 59–63), would allow the binding of the RD3-GCAP1 complex to the target GC1.

3.5. Functional implications of the RD3d-GCAP1 interaction

Previous results suggested a complex scenario for the inhibition of GC1 by RD3d and GCAP1, as the inhibitory activity was observed both in the presence and absence of GCAP1 (Fig. 1C), at both high and low Ca^{2+} concentrations. However, while at high Ca^{2+} GC1 inhibition occurred through a direct interaction with GCAP1, under low Ca^{2+}, when GCAP1 is Mg^{2+}-bound and thus in its activating form, RD3d was the only responsible for GC1 inhibition through one of its binding interfaces [34]. Given that: i) pathological GCAP1 variants associated with IRDs appear to interact with RD3d independently of the specific mutation (except for E111V); and ii) the pathological mechanism of IRD-associated GCAP1 variants is GC1 dysregulation, we tested the inhibitory potential of RD3d in the presence of the GCAP1 mutants (Fig. 6).

Activity assays with GCAP1 variants in the absence of RD3d are shown in Fig. 6A. While GC1 maximal activation was essentially unaffected under conditions mimicking illuminated photoreceptors (low Ca^{2+}), all IRD-associated GCAP1 variants led to constitutive enzymatic activation under conditions corresponding to dark-adapted photoreceptors, in line with previous observations [10,11,13]. Indeed, under high Ca^{2+} conditions, pathological variants failed to fully inhibit GC1, which retained approximately 33% of its maximal activity in the mildest case (N104H) and up to 60% in the most severe (E111V), thus leading to continuous production of cGMP, which is known to drive photoreceptor cell death [35]. Strikingly, the addition of RD3d to the GCAP1-GC1 system strongly inhibited GC1 activation and restored basal activity levels in all tested cases (Fig. 6B), including E111V-GCAP1 which did not interact with RD3d (Fig. 2 and Fig. 3B), in line with the presence of a second RD3d binding interface with GC1 [34]. Overall, even relatively low amounts of RD3d are apparently capable of counteracting the dysregulation of GC1 induced by all tested IRD-associated GCAP1 variants, when proteins are found in proximity.

Comparative analysis of X-fold activation confirmed these observations (Fig. 6C, D; Table 3). In the absence of RD3d, WT-GCAP1 displayed an X-fold of 39.9 ± 11.3, whereas all pathological variants showed dramatically reduced values ranging from 0.7 ± 0.1 (E111V) to 3.8 ± 0.1 (N104H) (Fig. 6C, Table 3). Upon RD3d addition, the X-fold of WT-GCAP1 decreased to 6.0 ± 1.4, indicating that RD3d modulates GC1 activity even under physiological regulation. All variants converged to similarly low values (Fig. 6D, Table 3), which further supports the notion that RD3d mitigates the dysregulation of GC1 activity induced by IRD-associated GCAP1 mutations.

3.6. Cellular localization of RD3, GCAP1 and GC1

Previous data suggested that specific and not mutually exclusive interactions between GCAP1, RD3 and GC1 may occur under different conditions, including varying local Ca^{2+} concentrations. To investigate the *in vivo* relevance of this concept, we performed

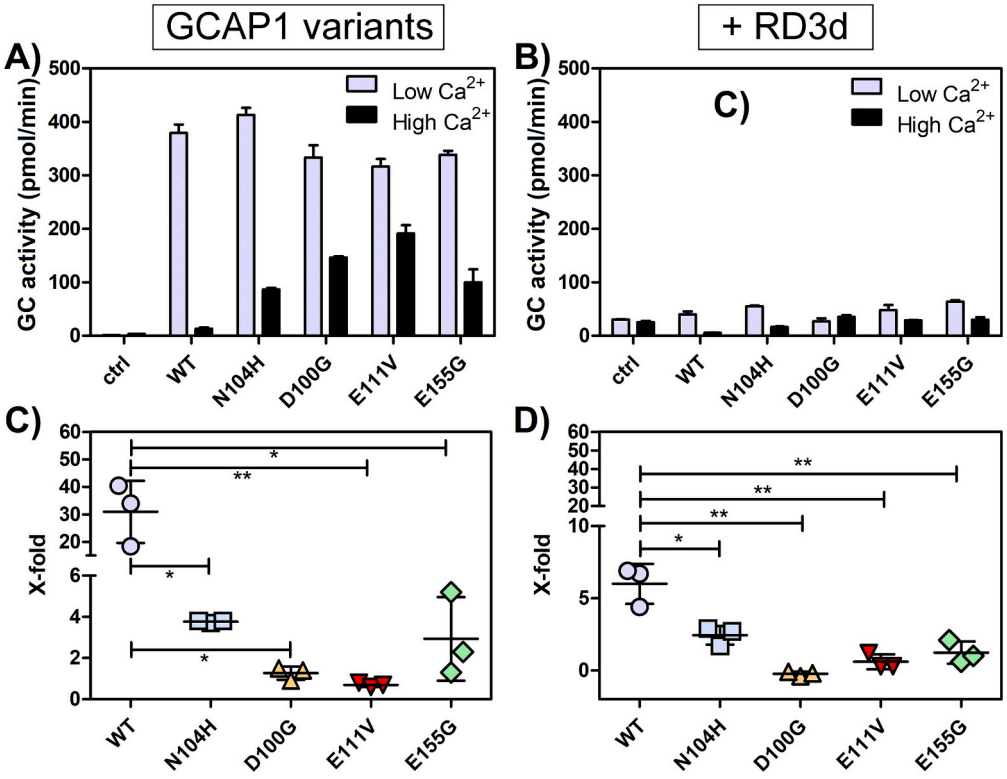

Fig. 6. Effects of RD3d on GC1 regulation by IRD-associated GCAP1 variants. A) cGMP synthesis by GC1 was measured in the presence of 5 μM GCAP1 variants WT, N104H, D100G, E111V, and E155G in the absence and B) in the presence of 200 nM RD3d. C) X-fold values relative to GC1 regulation by GCAP1 variants WT (grey circles), N104H (cyan squares), D100G (orange upward triangles), E111V (red downward triangles), and E155G (green diamonds) in the absence and D) in the presence of 200 nM RD3d. The GC1 activity is shown as pmol of cGMP produced per minute of reaction, data are reported as average ± standard deviation of three technical replicates. X-fold was calculated as follows: $((GC1^{low\_Ca2+}\text{-}GC^{high\_Ca2+})/GC^{high\_Ca2+})$. The statistical significance of the differences was assessed by two-tailed Student's t-test with a significance threshold of $p < 0.05$, the number of asterisks represents the p-value: * for $p < 0.05$ and ** for $p < 0.01$.

Table 3
X-fold variations in the absence or presence of RD3d.

	WT	N104H	D100G	E111V	E155G
-RD3d	39.9 ± 11.3	3.8 ± 0.1	1.3 ± 0.3	0.7 ± 0.1	2.9 ± 2.0
+ RD3d	6.0 ± 1.4	2.4 ± 0.6	0.3 ± 0.2	0.6 ± 0.5	1.3 ± 0.8

immunohistochemical analysis on retinal sections from wild-type C57BL/6J mice at postnatal day 30 (P30) (Fig. 7), when retinal development is complete and photoreceptor circuits are fully mature [36].

RD3 immunoreactivity was weakly detected in the photoreceptor outer segments (OS), while predominant localization was observed in the photoreceptor inner segments (IS) (Fig. 7A). Additionally, RD3 was present in the outer plexiform layer (OPL), displaying a punctate pattern. On the other hand, GCAP1 exhibited a more extensive distribution compared to RD3 (Fig. 7B), with robust signals detected throughout both the IS and OS of photoreceptors, while punctate labeling was also observed in the OPL, consistent with synaptic localization. GC1 immunoreactivity was detected in both the outer and inner photoreceptor layers (Fig. 7C). In the outer photoreceptor region, signal intensity was slightly reduced due to partial loss of the retinal pigment epithelium during tissue processing. In contrast to the punctate pattern of RD3 and GCAP1, GC1 displayed a diffuse, homogeneous labeling across the OPL, possibly reflecting a broader membrane distribution.

The overlapping distribution patterns of RD3, GCAP1, and GC1 in the

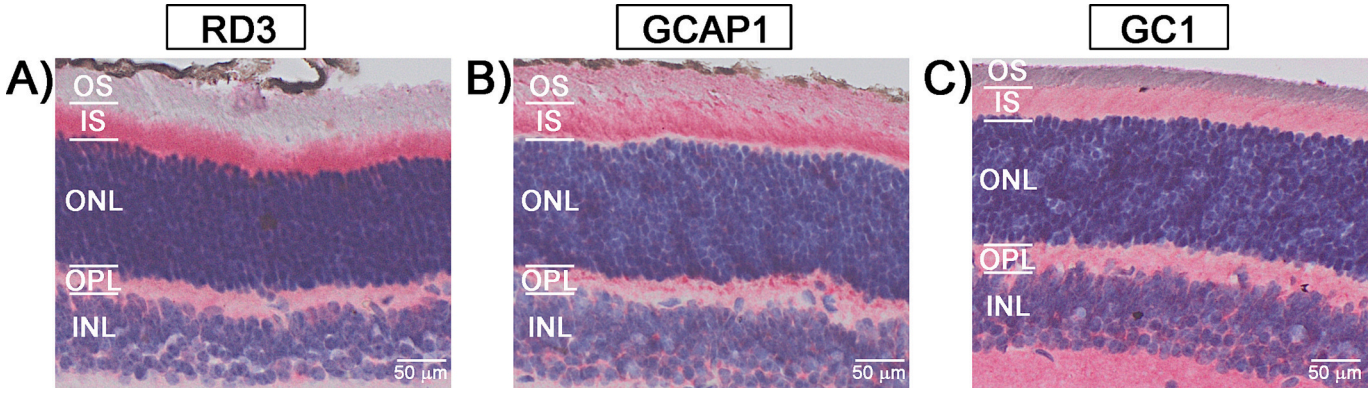

Fig. 7. Immunohistochemical staining of retinal sections from C57BL/6J wild-type mice at P30. Representative images showing A) RD3, B) GCAP1, and C) GC1 immunolabeling. Images were acquired with an Evident APEX microscope (20× objective) from 4 independent animals. Scale bar: 50 μm.

photoreceptor inner segments and synaptic terminals within the OPL are consistent with the possibility that these proteins may physically interact to form a functional complex involved in regulating guanylate cyclase activity. However, the predominantly weak RD3 signal in the OS, where GCAP1 and GC1 are instead robustly expressed, suggests that the RD3-GCAP1 interaction may occur primarily in the inner segment and synaptic terminals rather than in the outer segment. The formation of a direct RD3-GCAP1 complex and its functional interplay with GC1 may thus depend on the specific cellular compartment and local Ca^{2+} concentration.

4. Discussion

The present study provides a comprehensive biochemical and structural characterization of the interaction between RD3 and GCAP1, two key regulators of retinal GC1, and explores its functional implications in the context of inherited retinal dystrophies (IRDs).

4.1. Ca^{2+}-dependence of the GCAP1-RD3 interaction and physiological implications

Our NMR and SPR data demonstrate that the interaction between RD3d and GCAP1 is strongly dependent on Ca^{2+}. While a modest interaction was detected under Mg^{2+}-only conditions, Ca^{2+} binding to GCAP1 dramatically enhanced both the extent and affinity of complex formation, reaching physiologically relevant values ($K_D \sim 1.6$ μM). This observation must be interpreted considering the highly compartmentalized nature of Ca^{2+} homeostasis in photoreceptors. In the outer segment, cytoplasmic Ca^{2+} concentration ranges between 300 and 500 nM in darkness and drops to 20–50 nM in rods or < 10 nM in cones upon saturating light exposure, as extensively documented in vertebrate photoreceptors [37]. Similar values have been reported in mammalian rods, with dark $Ca^{2+} \sim 250$ nM decreasing to ~ 23 nM in light [38]. However, the photoreceptor inner segment and synaptic terminal exhibit markedly different Ca^{2+} dynamics: the ellipsoid region maintains Ca^{2+} levels around 750 nM, while the synaptic terminal reaches $\sim$ 2 μM in darkness (depolarized state) and decreases to ~ 50 nM during light adaptation (hyperpolarized state), spanning an overall dynamic range of approximately 40-fold [39]. Importantly, these Ca^{2+} concentration ranges have been documented across multiple vertebrate species including amphibians and mammals, suggesting conserved mechanisms that are likely relevant to human photoreceptors as well.

In this context, our immunohistochemical data reveal a predominantly weak RD3 signal in the outer segment, where GCAP1 and GC1 are robustly expressed. This suggests that an RD3-GCAP1-GC1 ternary complex may not form primarily in this compartment. Rather, the strong co-localization of all three proteins in the inner segment and synaptic terminals—compartments characterized by higher and more variable Ca^{2+} concentrations—points to these regions as the likely sites of RD3-GCAP1 complex formation and functional interplay (Fig. 8). The high Ca^{2+} levels in the synaptic terminal ($\sim$ 2 μM in darkness) would strongly favor the Ca^{2+}-bound state of GCAP1 and consequently its high-affinity interaction with RD3, consistent with our biochemical observations. Notably, the punctate pattern of RD3 and GCAP1 immunoreactivity in the OPL, in contrast to the more diffuse GC1 distribution, suggests that RD3-GCAP1 complexes may be concentrated in specific microdomains within the synaptic terminal. Given that the exocytotic Ca^{2+} sensor in photoreceptor ribbon synapses displays an unusually high Ca^{2+} affinity with a threshold of $\sim$ 400 nM and low cooperativity [40], the local regulation of Ca^{2+} signaling in this compartment is particularly critical for proper neurotransmitter release. The formation of RD3-GCAP1-GC1 complexes in synaptic terminals may therefore contribute to the fine-tuning of cGMP levels in this functionally specialized domain.

These findings align remarkably well with the model proposed by Peshenko, Dizhoor and colleagues for the physiological role of RD3 [15,41]. According to this model, RD3 functions to block GC1 activity during its trafficking from the inner segment to the outer segment, preventing premature cGMP synthesis before the cyclase reaches its functional destination in the disk membranes. Our demonstration that the GCAP1-RD3 interaction is Ca^{2+}-dependent provides a molecular explanation for how this regulatory mechanism could be spatially controlled: the steep Ca^{2+} gradient across the connecting cilium, with higher concentrations in the inner segment and lower concentrations in the outer segment, would act as a biochemical "gate" that promotes RD3-GCAP1 complex formation in the inner segment while disfavoring it in the outer segment. In this scenario, as the RD3-GCAP1-GC1 complex traffics toward the outer segment and encounters progressively lower Ca^{2+} concentrations, the reduced Ca^{2+} occupancy of GCAP1 would weaken its interaction with RD3, facilitating dissociation and allowing GCAP1 to assume its physiological role as a Ca^{2+}-dependent regulator of GC1 activity in the disk membranes. The finding that Mg^{2+}-bound GCAP1 retains a weak but detectable interaction with RD3d, as evidenced by NMR chemical shift perturbations and by SPR, suggests that even under light-adapted conditions some degree of RD3-GCAP1 association may persist. This could provide a mechanism for rapid reassembly of the inhibitory complex upon return to darkness, when Ca^{2+} levels rise again.

4.2. Structural insights into the GCAP1-RD3 interface

A structural model of the GCAP1-RD3 complex obtained by AlphaFold3 (Fig. 5), validated against NMR chemical shift perturbation data, reveals that the interaction interface mainly involves residues in the N-terminal region of GCAP1 (residues H19, K23, M26, M74, V77, A78) that contact exposed residues in RD3 (M24, L29, H89, C93, G94, L98). The AlphaFold3 model of GCAP1-RD3 also suggests that N-terminal residues of RD3 (residues 1–12) form an α-helix that contacts a cleft between EF2 and EF3 in GCAP1. This N-terminal contact by RD3 predicts that GCAP1 might bind to full-length RD3 with higher affinity than RD3d. However, our SPR studies indicate that GCAP1 binds with similar affinity to both RD3 and RD3d (Table 1). So, the N-terminal helix of RD3 (residues 1–12) predicted by AlphaFold3 has not been experimentally verified and future studies are needed to further test whether the RD3 N-terminal helix interacts with GCAP1.

It is noteworthy that, besides being consistent with NMR data, the proposed structural model (Fig. 5) predicts that Ca^{2+}-bound GCAP1 interacts with RD3 via residues that are involved in both GCAP1 dimerization [5] and GC1 interaction [31]. This points to a complex molecular scenario in which both GCAP1 and RD3 might bind to GC1 as separate binary complexes and independently of each other. In particular, the GCAP1 binding site residues that contact RD3 (Fig. 5) are the same GCAP1 residues that contact GC1, and the RD3 residues that contact GCAP1 are the same that contact GC1. This could imply that GC1 binding might cause the GCAP1-RD3 complex to dissociate. However, the fact that RD3 contacts many of the residues in GCAP1 (H19, K23, M26, M74, V77, A78, W94) shown previously to contact GC1 during cyclase activation [31] also suggests that RD3 may block GCAP1 activation of GC1 by altering how GCAP1 binds to GC1. For example, we propose that the RD3-GCAP1 complex may bind to GC1 at an interface that is different from the site that binds to Mg^{2+}-bound GCAP1 during cyclase activation (Fig. 8). This distinct binding of RD3-GCAP1 to GC1 might stabilize the inactive conformation of GC1 and therefore explain how the cyclase activity is selectively inhibited at high Ca^{2+} levels. This model expands the regulatory capability of the cyclase by potentially enabling the formation of higher-order supramolecular assemblies with distinct functional properties.

4.3. Effects of IRD-associated mutations on the GCAP1-RD3 recognition

A striking finding of our study is that the IRD-associated variant E111V-GCAP1 completely abolishes the interaction with RD3d under both Ca^{2+} and Mg^{2+} conditions, as demonstrated by NMR and SPR

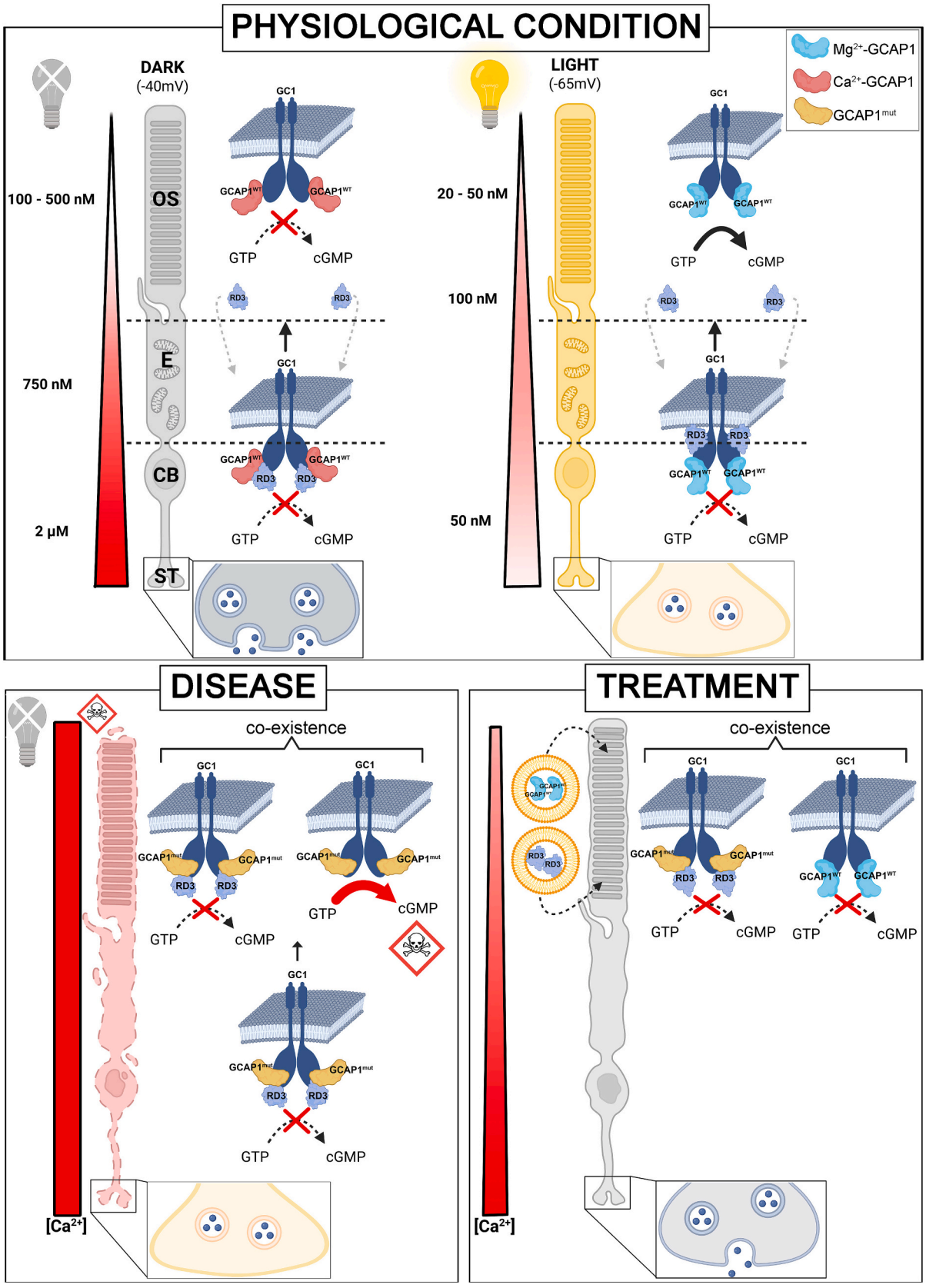

(caption on next page)

Fig. 8. Model of GCAP1-RD3-GC1 interaction under physiological and pathological conditions. Under physiological conditions (PHYSIOLOGICAL CONDITION), dark-adapted photoreceptors exhibit a Ca^{2+} gradient that decreases from the synaptic terminal (ST, 2 μM) through the ellipsoid (E, 750 nM) to the outer segment (OS, 100–500 nM) [39]. In the cell body (CB), under high Ca^{2+} concentrations, GC1 is inhibited by both Ca^{2+}-bound GCAP1 (red) and RD3. During translocation toward the OS, decreasing Ca^{2+} levels induce RD3 dissociation, leaving GC1 inhibited solely by Ca^{2+}-bound GCAP1. Following light absorption, the rapid Ca^{2+} decrease leads to GC1 activation by Mg^{2+}-bound GCAP1 (blue) in the OS, while in the CB, cGMP production remains inhibited directly by RD3 in a Ca^{2+}- and GCAP1-independent manner. Under pathological conditions (DISEASE), IRD-associated GCAP1 mutations ($GCAP1^{mut}$, yellow) cause an imbalance in Ca^{2+} and cGMP concentrations due to constitutive GC1 activation, with loss of the Ca^{2+} gradient and progressive cellular accumulation. In the CB, GC1 inhibition is mediated by the $GCAP1^{mut}$-RD3 complex (except for E111V), while in the OS two states coexist: cGMP overproduction due to loss of Ca^{2+}-dependent GC1 inhibition by $GCAP1^{mut}$, and RD3-mediated inhibition favored by elevated local Ca^{2+} concentrations that prevent its dissociation in the ellipsoid. This coexistence may explain the slow but progressive degeneration and suggests a potential mutation-independent therapeutic approach (TREATMENT), consisting of liposome-mediated delivery of recombinant i) WT-GCAP1 [43] to compensate for haploinsufficiency, or ii) RD3d to block the constitutively activated GC1, ultimately reestablishing the Ca^{2+} gradient and slowing degeneration. Created in BioRender. Dell'Orco, D. (2026) https://BioRender.com/0arrlt7, https://BioRender.com/78ldt2z.

experiments. E111 is located in the EF3 Ca^{2+}-binding loop and its substitution with valine induces local conformational changes [10] that propagate to the entire RD3 recognition interface. This observation has important pathological implications: in patients carrying the E111V mutation, the loss of RD3-GCAP1 interaction may exacerbate GC1 dysregulation by removing an additional layer of cyclase inhibition in the inner segment and synaptic terminal. Hints on the effects of the dysregulation of the GCAP1-GC1 complex further propagating to the synaptic terminal were previously reported by some of us in a study where the GCAP1 double mutant N104H-G105R resulted in a patient showing abnormal electroretinogram with significant alteration of the ON-pathway related to the b-wave generation [42].

Kinetic analysis of IRD-associated GCAP1 variants revealed differential effects on the association and dissociation processes. Interestingly, E155G-GCAP1, the only IRD-associated variant in this study located in the EF4 motif, showed a 3-fold increase in k^{on} compared to WT [$(7.4 \pm 3.5) \times 10^3$ vs $(2.4 \pm 1.2) \times 10^3$ M^{-1} s^{-1}], ultimately resulting in a 2.8-fold increase in affinity ($K_D = 450 \pm 230$ nM). An allosteric mechanism connecting EF4 with the N-terminal domain, and specifically with EF1, EF2, and the region at the interface with the myristoyl moiety, has been proposed by exhaustive molecular dynamics simulations [27] and confirmed by experimental studies [28]. The E155G mutation might therefore induce conformational changes in the EF4 region, which are transmitted to the N-terminal domain. The observed effect on k^{on} combined with the predicted model of RD3-GCAP1 interaction suggests that the perturbation induced by the substitution propagates through long-range allosteric effects that favorably affect the association process.

4.4. Dual mechanism of GC1 inhibition by RD3 and therapeutic implications

Functional assays revealed that RD3d inhibits GC1 activity even in the presence of E111V-GCAP1, which does not interact with RD3. This observation provides strong evidence for the existence of a direct RD3 binding site on GC1, independent of GCAP1, consistent with the biochemical characterization by Peshenko and colleagues [15–17,34]. The dual mechanism of GC1 inhibition by RD3—both direct and GCAP1-mediated—may serve as a fail-safe system to ensure proper cyclase regulation under varying physiological conditions and in different photoreceptor compartments, where local Ca^{2+} concentrations differ substantially (Fig. 8). An important finding of this study is that RD3d effectively mitigates GC1 dysregulation induced by all tested IRD-associated GCAP1 variants. In the absence of RD3d, pathological variants displayed dramatically reduced X-fold values compared to wild-type, reflecting their failure to properly inhibit GC1 under high Ca^{2+} conditions—a feature that leads to constitutive cGMP production and photoreceptor cell death [35]. Strikingly, RD3d addition essentially abolished the functional differences among all mutants, restoring near-basal GC1 activity regardless of the specific mutation. This mutation-independent effect has potentially transformative therapeutic implications. Current gene therapy approaches for GCAP1-associated retinopathies would require mutation-specific interventions, given the dominant nature of these disorders and the need to either correct or silence the mutant allele. In contrast, our data suggest that RD3 delivery, potentially combined with wild-type GCAP1, could provide a unified therapeutic strategy effective across multiple GCAP1 mutations by acting downstream of the primary defect, directly counteracting GC1 hyperactivity.

We have recently demonstrated the feasibility of delivering recombinant proteins to photoreceptors using liposome-mediated approaches [22] and validated their functional integration in retinal organotypic cultures [43]. This protein replacement strategy, schematically illustrated in Fig. 8, bypasses several limitations of gene therapy, including immune responses, insertional mutagenesis, and challenges in achieving appropriate expression levels. The present findings, showing that even low concentrations of RD3d (200 nM) are sufficient to counteract pathological GC1 activation, support the potential therapeutic relevance of this approach.

4.5. Open questions and future directions

Several questions remain open, including experimental validation of the RD3-GCAP1 structural model by complementary biophysical techniques, and quantification of the relative contributions of direct RD3-GC1 versus RD3-GCAP1-mediated inhibition under different physiological conditions. Furthermore, determining whether the Ca^{2+}-dependent dissociation of the RD3-GCAP1 complex occurs with kinetics compatible with the trafficking time through the connecting cilium will be essential to fully validate the proposed model.

Notably, our findings may have implications beyond the visual system. RD3 has recently been shown to inhibit membrane-bound guanylate cyclases activated by natriuretic peptides (GC-A and GC-B) in brain tissue, including cerebellum, hippocampus, neocortex, and astrocytes, with inhibitory constants in the nanomolar range [44]. This suggests that RD3 may function as a general regulator of membrane guanylate cyclase activity across different tissues and signaling contexts. Furthermore, RD3 expression has been found to be downregulated in glioblastoma compared to non-tumor brain tissue, and its overexpression in cell culture systems significantly decreases cell viability, induces cell-cycle arrest at the G2/M phase, and promotes apoptosis [45]. These observations point to a potential tumor suppressor role for RD3 and suggest that the supramolecular complexes involving RD3, GCAPs, and guanylate cyclases may participate in cellular processes extending well beyond phototransduction, including cell cycle regulation and survival pathways. The broader physiological and pathophysiological significance of these interactions warrants further investigation.

5. Conclusions

In summary, this study establishes RD3 as a Ca^{2+}-dependent modulator of GCAP1 function and identifies a dual mechanism of GC1 inhibition involving both direct and GCAP1-mediated interactions. The Ca^{2+}-dependence of the GCAP1-RD3 interaction provides a molecular rationale for the spatial regulation of this complex along the photoreceptor compartments, with the Ca^{2+} gradient across the connecting cilium acting as a biochemical switch that promotes complex formation

in the inner segment while facilitating dissociation in the outer segment. This mechanism is fully consistent with the proposed role of RD3 in preventing premature GC1 activation during trafficking. The mutation-independent rescue of GC1 dysregulation by RD3d opens new avenues for protein-based therapeutic approaches in GCAP1-associated inherited retinal dystrophies.

CRediT authorship contribution statement

Valerio Marino: Writing – original draft, Software, Methodology, Investigation. **Effibe O. Ahoulou:** Investigation, Formal analysis, Data curation. **Giuditta Dal Cortivo:** Writing – original draft, Visualization, Methodology, Investigation. **Anna Avesani:** Writing – original draft, Methodology, Investigation. **James B. Ames:** Writing – review & editing, Writing – original draft, Supervision, Formal analysis. **Daniele Dell'Orco:** Writing – review & editing, Writing – original draft, Supervision, Funding acquisition, Formal analysis, Conceptualization.

Declaration of competing interest

The authors declare that they have no known competing financial interests or personal relationships that could have appeared to influence the work reported in this paper.

Acknowledgments

The Centro Piattaforme Tecnologiche of the University of Verona is acknowledged for providing access to the spectroscopic platform. This study was supported by the Next Generation EU/Ministry of University and Research project: “A multiscale integrated approach to the study of the nervous system in health and disease (MNESYS)”, CUP B33C22001060002, PE00000006 missione 4, componente 2, investimento 1.3. Dr. Amedeo Biasi is gratefully acknowledged for performing molecular docking simulations.

Data availability

Data will be made available on request.

References

[1] K.-W. Koch, D. Dell’Orco, Protein and signaling networks in vertebrate photoreceptor cells, Front. Mol. Neurosci. 8 (2015).
[2] A.M. Dizhoor, E.V. Olshevskaya, I.V. Peshenko, Mg2+/Ca2+ cation binding cycle of guanylyl cyclase activating proteins (GCAPs): role in regulation of photoreceptor guanylyl cyclase, Mol. Cell. Biochem. 334 (1–2) (2009) 117–124.
[3] R. Stephen, G. Bereta, M. Golczak, K. Palczewski, M.C. Sousa, Stabilizing function for myristoyl group revealed by the crystal structure of a neuronal calcium sensor, guanylate cyclase-activating protein 1, Structure 15 (11) (2007) 1392–1402.
[4] J.B. Ames, Dimerization of neuronal calcium sensor proteins, Front. Mol. Neurosci. 11 (2018).
[5] F. Bonì, V. Marino, C. Bidoia, E. Mastrangelo, A. Barbiroli, D. Dell’Orco, M. Milani, Modulation of guanylate cyclase activating protein 1 (GCAP1) dimeric assembly by Ca2+ or Mg2+: hints to understand protein activity, Biomolecules 10 (10) (2020) 1408.
[6] A. Biasi, V. Marino, G. Dal Cortivo, D. Dell’Orco, Supramolecular complexes of GCAP1: implications for inherited retinal dystrophies, Int. J. Biol. Macromol. 279 (2024) 135068.
[7] P. Behnen, D. Dell’Orco, K.-W. Koch, Involvement of the calcium sensor GCAP1 in hereditary cone dystrophies, Biol. Chem. 391 (6) (2010).
[8] D. Dell’Orco, P. Behnen, S. Linse, K.-W. Koch, Calcium binding, structural stability and guanylate cyclase activation in GCAP1 variants associated with human cone dystrophy, Cell. Mol. Life Sci. 67 (6) (2010) 973–984.
[9] V. Marino, A. Scholten, K.-W. Koch, D. Dell’Orco, Two retinal dystrophy-associated missense mutations inGUCA1Awith distinct molecular properties result in a similar aberrant regulation of the retinal guanylate cyclase, Hum. Mol. Genet. 24 (23) (2015) 6653–6666.
[10] V. Marino, G. Dal Cortivo, E. Oppici, P.E. Maltese, F. D’Esposito, E. Manara, L. Ziccardi, B. Falsini, A. Magli, M. Bertelli, D. Dell’Orco, A novel p.(Glu111Val) missense mutation in *GUCA1A* associated with cone-rod dystrophy leads to impaired calcium sensing and perturbed second messenger homeostasis in photoreceptors, Hum. Mol. Genet. 27 (24) (2018) 4204–4217.
[11] A. Biasi, V. Marino, G. Dal Cortivo, P.E. Maltese, A.M. Modarelli, M. Bertelli, L. Colombo, D. Dell’Orco, A novel GUCA1A variant associated with cone dystrophy alters cGMP signaling in photoreceptors by strongly interacting with and Hyperactivating retinal guanylate cyclase, Int. J. Mol. Sci. 22 (19) (2021) 10809.
[12] S.E. Wilkie, Y. Li, E.C. Deery, R.J. Newbold, D. Garibaldi, J.B. Bateman, H. Zhang, W. Lin, D.J. Zack, S.S. Bhattacharya, M.J. Warren, D.M. Hunt, K. Zhang, Identification and functional consequences of a new mutation (E155G) in the gene for GCAP1 that causes autosomal dominant cone dystrophy, Am. J. Hum. Genet. 69 (3) (2001) 471–480.
[13] G. Dal Cortivo, V. Marino, F. Bonì, M. Milani, D. Dell'Orco, Missense mutations affecting Ca2+-coordination in GCAP1 lead to cone-rod dystrophies by altering protein structural and functional properties, Biochim. Biophys. Acta 1867 (10) (2020) 118794.
[14] S. Azadi, L.L. Molday, R.S. Molday, RD3, the protein associated with Leber congenital amaurosis type 12, is required for guanylate cyclase trafficking in photoreceptor cells, Proc. Natl. Acad. Sci. 107 (49) (2010) 21158–21163.
[15] I.V. Peshenko, E.V. Olshevskaya, S. Azadi, L.L. Molday, R.S. Molday, A.M. Dizhoor, Retinal degeneration 3 (RD3) protein inhibits catalytic activity of retinal membrane guanylyl cyclase (RetGC) and its stimulation by activating proteins, Biochemistry 50 (44) (2011) 9511–9519.
[16] I.V. Peshenko, E.V. Olshevskaya, A.M. Dizhoor, Functional study and mapping sites for interaction with the target enzyme in retinal degeneration 3 (RD3) protein, J. Biol. Chem. 291 (37) (2016) 19713–19723.
[17] I.V. Peshenko, Q. Yu, S. Lim, D. Cudia, A.M. Dizhoor, J.B. Ames, Retinal degeneration 3 (RD3) protein, a retinal guanylyl cyclase regulator, forms a monomeric and elongated four-helix bundle, J. Biol. Chem. 294 (7) (2019) 2318–2328.
[18] J.S. Friedman, B. Chang, C. Kannabiran, C. Chakarova, H.P. Singh, S. Jalali, N. L. Hawes, K. Branham, M. Othman, E. Filippova, D.A. Thompson, A.R. Webster, S. Andréasson, S.G. Jacobson, S.S. Bhattacharya, J.R. Heckenlively, A. Swaroop, Premature truncation of a novel protein, RD3, exhibiting subnuclear localization is associated with retinal degeneration, Am. J. Hum. Genet. 79 (6) (2006) 1059–1070.
[19] R. Zulliger, M.I. Naash, R.V.S. Rajala, R.S. Molday, S. Azadi, Impaired Association of Retinal Degeneration-3 with guanylate Cyclase-1 and guanylate cyclase-activating Protein-1 leads to Leber congenital Amaurosis-1, J. Biol. Chem. 290 (6) (2015) 3488–3499.
[20] J.-Y. Hwang, K.-W. Koch, Calcium- and Myristoyl-dependent properties of guanylate cyclase-activating Protein-1 and Protein-2, Biochemistry 41 (43) (2002) 13021–13028.
[21] M.M. Bradford, A rapid and sensitive method for the quantitation of microgram quantities of protein utilizing the principle of protein-dye binding, Anal. Biochem. 72 (1–2) (1976) 248–254.
[22] S. Asteriti, V. Marino, A. Avesani, A. Biasi, G. Dal Cortivo, L. Cangiano, D. Dell’Orco, Recombinant protein delivery enables modulation of the phototransduction cascade in mouse retina, Cell. Mol. Life Sci. 80 (12) (2023).
[23] F. Delaglio, S. Grzesiek, G.W. Vuister, G. Zhu, J. Pfeifer, A. Bax, NMRPipe: a multidimensional spectral processing system based on UNIX pipes, J. Biomol. NMR 6 (3) (1995) 277–293.
[24] J. Abramson, J. Adler, J. Dunger, R. Evans, T. Green, A. Pritzel, O. Ronneberger, L. Willmore, A.J. Ballard, J. Bambrick, S.W. Bodenstein, D.A. Evans, C.-C. Hung, M. O’Neill, D. Reiman, K. Tunyasuvunakool, Z. Wu, A. Žemgulytė, E. Arvaniti, C. Beattie, O. Bertolli, A. Bridgland, A. Cherepanov, M. Congreve, A.I. Cowen-Rivers, A. Cowie, M. Figurnov, F.B. Fuchs, H. Gladman, R. Jain, Y.A. Khan, C.M. R. Low, K. Perlin, A. Potapenko, P. Savy, S. Singh, A. Stecula, A. Thillaisundaram, C. Tong, S. Yakneen, E.D. Zhong, M. Zielinski, A. Žídek, V. Bapst, P. Kohli, M. Jaderberg, D. Hassabis, J.M. Jumper, Accurate structure prediction of biomolecular interactions with AlphaFold 3, Nature 630 (8016) (2024) 493–500.
[25] C. Chen, K. Nakatani, Y. Koutalos, Free magnesium concentration in salamander photoreceptor outer segments, J. Physiol. 553 (1) (2003) 125–135.
[26] V. Marino, S. Sulmann, K.-W. Koch, D. Dell'Orco, Structural effects of Mg2+ on the regulatory states of three neuronal calcium sensors operating in vertebrate phototransduction, Biochim. Biophys. Acta 1853 (9) (2015) 2055–2065.
[27] V. Marino, D. Dell’Orco, Allosteric communication pathways routed by Ca2+/Mg2+ exchange in GCAP1 selectively switch target regulation modes, Sci. Rep. 6 (1) (2016).
[28] I.V. Peshenko, E.V. Olshevskaya, S. Lim, J.B. Ames, A.M. Dizhoor, Calcium-Myristoyl tug is a new mechanism for intramolecular tuning of calcium sensitivity and target enzyme interaction for guanylyl cyclase-activating protein 1, J. Biol. Chem. 287 (17) (2012) 13972–13984.
[29] O. Keskin, B.G. Pierce, Y. Hourai, Z. Weng, Accelerating protein docking in ZDOCK using an advanced 3D convolution library, PLoS One 6 (9) (2011) e24657.
[30] D. Kozakov, R. Brenke, S.R. Comeau, S. Vajda, PIPER: an FFT-based protein docking program with pairwise potentials, Proteins 65 (2) (2006) 392–406.
[31] I.V. Peshenko, E.V. Olshevskaya, S. Lim, J.B. Ames, A.M. Dizhoor, Identification of target binding site in photoreceptor guanylyl cyclase-activating protein 1 (GCAP1), J. Biol. Chem. 289 (14) (2014) 10140–10154.
[32] A. Schrem, C. Lange, M. Beyermann, K.-W. Koch, Identification of a domain in guanylyl cyclase-activating protein 1 that interacts with a complex of guanylyl cyclase and tubulin in photoreceptors, J. Biol. Chem. 274 (10) (1999) 6244–6249.
[33] K.-W. Koch, S. Lim, I.V. Peshenko, A.M. Dizhoor, J.B. Ames, Structural insights for activation of retinal guanylate cyclase by GCAP1, PLoS One 8 (11) (2013) e81822.
[34] I.V. Peshenko, A.M. Dizhoor, Two clusters of surface-exposed amino acid residues enable high-affinity binding of retinal degeneration-3 (RD3) protein to retinal guanylyl cyclase, J. Biol. Chem. 295 (31) (2020) 10781–10793.

[35] M. Power, S. Das, K. Schütze, V. Marigo, P. Ekström, F. Paquet-Durand, Cellular mechanisms of hereditary photoreceptor degeneration – focus on cGMP, Prog. Retin. Eye Res. 74 (2020) 100772.
[36] M. Völkner, T. Kurth, J. Schor, L.J.A. Ebner, L. Bardtke, C. Kavak, J. Hackermüller, M.O. Karl, Mouse retinal organoid growth and maintenance in longer-term culture, Front. Cell Dev. Biol. 9 (2021).
[37] D. Krizaj, Calcium regulation in photoreceptors, Front. Biosci. 7 (4) (2002) d2023–d2044.
[38] M.L. Woodruff, A.P. Sampath, H.R. Matthews, N.V. Krasnoperova, J. Lem, G. L. Fain, Measurement of cytoplasmic calcium concentration in the rods of wild-type and transducin knock-out mice, J. Physiol. 542 (3) (2002) 843–854.
[39] T. Szikra, D. Križaj, The dynamic range and domain-specific signals of intracellular calcium in photoreceptors, Neuroscience 141 (1) (2006) 143–155.
[40] W.B. Thoreson, K. Rabl, E. Townes-Anderson, R. Heidelberger, A highly Ca2+-sensitive pool of vesicles contributes to linearity at the rod photoreceptor ribbon synapse, Neuron 42 (4) (2004) 595–605.
[41] A.M. Dizhoor, I.V. Peshenko, Regulation of retinal membrane guanylyl cyclase (RetGC) by negative calcium feedback and RD3 protein, Pflugers Arch. - Eur. J. Physiol. 473 (9) (2021) 1393–1410.
[42] V. Marino, G. Dal Cortivo, P.E. Maltese, G. Placidi, E. De Siena, B. Falsini, M. Bertelli, D. Dell'Orco, Impaired Ca2+ sensitivity of a novel GCAP1 variant causes cone dystrophy and leads to abnormal synaptic transmission between photoreceptors and bipolar cells, Int. J. Mol. Sci. 22 (8) (2021) 4030.
[43] G. Dal Cortivo, C. Longo, B. Müller, A. Avesani, R. Pacchiana, M. Weller, V. Marino, L. Lytvynchuk, K. Stieger, D. Dell'Orco, Protein delivery to the eye: assessing therapeutic potential across inner and outer retina, Int. J. Pharm. 690 (2026) 126568.
[44] Y. Chen, A.U. Bräuer, K.-W. Koch, Retinal degeneration protein 3 controls membrane guanylate cyclase activities in brain tissue, Front. Mol. Neurosci. 15 (2022).
[45] Y. Chen, J. Hausmann, B. Zimmermann, S.O.A. Helgers, P. Dömer, J. Woitzik, U. Raap, N. Gray, A. Büttner, K.-W. Koch, A.U. Bräuer, Retinal degeneration protein 3 mutants are associated with cell-cycle arrest and apoptosis, Cell Death Dis. 11 (1) (2025).